Ethanol candle in enclosed environment:

Non-repeatability of measuring final

percent O_2

A Thesis Presented to

The Faculty of the Mathematics Program

California State University Channel Islands

In (Partial) Fulfillment

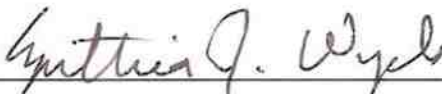of the Requirements for the Degree

Masters of Science

by

David Alan Bennett

December, 2011

Signature page for the Masters in Mathematics Thesis of David Alan Bennett

APPROVED FOR THE MATHEMATICS PROGRAM

_____ 12/9/11
Dr. Grégory Wood, Thesis Advisor   Date

_____ 12/9/11
Dr. Cynthia Wyels, Thesis Committee   Date

_____ 12/9/2011
Dr Geoffrey Buhl, Thesis Committee   Date

APPROVED FOR THE UNIVERSITY

_____ 12-9-11
Dr. Gary A. Berg, AVP Extended University   Date

© 2011

David Alan Bennett

To Lauren Uhler, for her patience, love, and support.

To my parents, Belinda Durham and Jim Bennett, and to my brothers,

Paul Bennett and Tommy Bennett.

In memory of Gregory McCauley, without whom a certain lack of

combustion equilibrium might have gone unnoticed.

Acknowledgements

This dissertation could not have been written without the constant advice and encouragement of my advisor, Gregory Wood. Many thanks must also go to the members of my committee, Cynthia Wyels and Geoffrey Buhl. I would also like to thank Raquel Baratta, Danika Lindsay, Luis Contreras, and Nick Avia. For support and encouragement throughout my time in graduate school, I would like to thank Cindy Enrique, Allison Chapin, Ken Lewis, Geoff Dougherty, Jorge Garcia, Jeffrey Gray, Nathan Roller, Paul Speigelhalter, and Byron Sturtevant. And to the many people, both in and out of academia and industry, who listened to the descriptions of this project, and who offered suggestion after suggestion, thank you.

Abstract

Ethanol candle in enclosed environment: Non-repeatability of measuring

final percent O_2

by David Alan Bennett

Paraffin wax tea light candles and ethanol-fuel candles are
ignited within an enclosed, plexiglass and glass environment
in an attempt to create a model of burn time before self-
extinction of various candles regardless of type, size, and the
volume and shape of the enclosed container. A lower limit of
final percent O_2 is found that is consistent with theory, but
these experiments do not always reach this limit, leading to
non-repeatability. Many factors, such as the relevant fluid
dynamical and flame dynamical systems, known combustion
models such as the those given by the National Institute
of Standards and Technology and the Boussinesq model of
buoyant combustion, and other current combustion studies
have been considered and controlled for without success.

CONTENTS

List of Figures

1. INTRODUCTION

Despite the general consensus that candles have been in use since the first century [1] the first real, comprehensive study of the physics of burning candles was conducted by Michael Faraday in 1861 [1][2]. More recent studies, however, have centered around more controlled flame and combustion situations, namely in an effort to detail specific types of small flame burn processes [2].

However, the National Institute of Standards and Technology (NIST) has noted a need to study simple candles and basic candle-like objects, specifically in support of fire investigation [2]. Reports from the National Candle Association note that candle use in homes has been increasing since the 1990s, with candles being used in 7 out of 10 homes, with retail candle sales exceeding approximately $2.3 billion with a 15% annual growth rate [2]. With the heightened use of candles, there has been an increase in candle-related fires and accidents. The US Consumer Product Safety Commission estimated that in 1998 there were 12800 candle-related fires that resulted in 1200 injuries and 170 deaths [2]. The National Fire Protection Association estimated that in 2001 there were 18,000 candle-related structure fires resulting in 1500 injuries, 190 deaths, and $265 Million in property loss and damage [2]. Another study in 2002 noted that unattended

candles were responsible for the majority of candle-related fires, followed by candles placed near combustible material [2]. Forty-five percent of candle-related fires were discovered to have originated in the bedroom, with the most common combustible materials being bedding, curtains, blinds and drapery [2].

Despite the trend of rising candle use and the subsequent rise in candle-related fires, there is very little information regarding candle flame dynamics and candle burning available to help fire investigators [2]. Instead, there is a trend, necessary in most cases, of studying other fire phenomena, such as general enclosure fires, pre-mixed fuel fires, reactant fires, microgravity fires, and even wildfire phenomena such as fire whirls and wildland-urban interface flame behavior [4][3][6]. The motivation for this thesis is not only rooted in the suggestion of further candle studies to help in fire prevention and investigation, but also in the field of flame and candle education.

The National Candle Association asserts that there are over 350 candle manufacturers in the United States alone, where a major manufacturer may offer between 1000 2000 types of candles [2]. Hamins et al. note that the most common type of candle in modern use is the petroleum-derived paraffin wax candle, specifically refined to contain a relatively low percentage of residual oil, although other candles may be manufactured from clear gels, stearic acid, and beeswax. Additives, such as dyes and fragrances, whose

actual experimental affect is uncertain, may be introduced to the wax, and are designed to not interfere with the actual burning of the candle, producing water and carbon dioxide as 'clean' combustion by-products. The most common type of wick is the cotton flat-braid wick, followed by the cored braid wick and square wick, with each type of wick designed to match the type of candle and wax being used [2].

As reported by the National Candle Association, common candle types include votive candles, column or pillar candles, taper candles, tea lights, luminaria, wax-filled or container candles, gel candles, floating candles, and speciality candles [2]. Votive candles, originally produced as white, unscented candles for religious purposes, are now produced with various dyes and scents. They are typically 50 mm to 60 mm high, 40 mm in diameter, and generally placed in a cup or glass container to collect the liquified wax. Column or pillar candles tend to be free-standing, rigid and thick, with varying heights and diameters. Taper candles are designed to be used in candle holders such as candelabra. They are typically slender, from 0.15 m to .45 m in height. Tea lights are typically 40 mm high and 25 mm in diameter, with the wax poured into its own metal container. Luminaria are so-called paper lanterns, typically used for outdoor purposes. They generally consist of a votive candle placed in a paper bag whose bottom has be filled with sand, or a small votive candle placed within a housing that has paper sides.

3

Wax-filled or container candles are candles made by pouring wax, usually dyed and scented, into a tin, special glass or pottery container. Gel candles are transparent, typically formed with a rubber-like consistency from gelled synthetic hydrocarbons or gelled mineral oils, poured into a container to hold its shape. Floating candles tend to be shallow candles with a convex bottom, designed to float in water. Speciality candles include shaped and free-standing candles, such as candles shaped and dyed to resemble, for example, Christmas decorations [2][7].

Paraffin wax is a mixture of straight-chain hydrocarbon molecules with a molecular formula of C_nH_{2n+2}, where $19 \leq n \leq 36$ with an average value of 25. Manufacturers determine the appropriateness of a particular paraffin wax, depending upon what type of candle they wish to fabricate, by physical properties that include the melting point, viscosity, odor, color, and oil content. Hamins et al. note that the most important physical property of paraffin wax to most manufacturers is the melting point, which dictates what type of candle can be made due to, for example, how fast the wax melts, how much liquid wax will collect, and how much wax can be present to begin with. Taper candles, for example, have a melting point of 59° to 65° C [2].

Despite the fact that heat release properties of paraffin wax, such as the effective heat of combustion, are not of general interest to candle manufactures, certain heat release properties are necessary to understand the characteristics of candle flames under laboratory conditions [2]. For example, the heat of combustion of burning wax is necessary to understand general behavior of a burning candle, and the heat release rate of a candle has a direct bearing on the candle's heat flux distribution [2][8].

The *effective heat release rate* of a candle flame, $\dot{Q}$, is given by

$$\dot{Q} = \chi_a \cdot \dot{m} \cdot H_c,$$

where $\dot{m}$ is the mass burning rate of the fuel, χ_a is the combustion efficiency, and H_c is the net heat of the complete combustion of the fuel [2]. Note that both $\dot{Q}$ and $\dot{m}$ are derivatives with respect to time, and by definition, $0 \leq \chi_a \leq 1$, varying for different fuels. Also,

$$\Delta h_{c,eff} = \chi_a \cdot H_c,$$

is the *effective heat of combustion*, so $\dot{Q}$ may be written as

$$\dot{Q} = \dot{m} \cdot \Delta h_{c,eff}.$$

The radiative heat loss fraction, χ_r, characterizes the radiative emission from a flame, influencing candle burning behavior. It is given by

$$\chi_r = \frac{\dot{Q}}{\dot{m} \cdot H_c},$$

where $\dot{Q}$ is the rate of radiative energy released to the surroundings, and the product $\dot{m} \cdot H_c$ is the heat release rate [2].

The physical properties of paraffin wax can be found throughout the literature. For example, the melting point is $48 - 68°$ C. The congealing point is $66-69°$ C. The flash point is $204-271°$ C. The fire point is $238-263°$ C. The boiling point is $350 - 430°$ C. The density at room temperature is $865-913$ kg/m^3. The kinematic viscosity at $100°$ C is $3.1-7.1$ mm^2/s. The vapor pressure at $100°$ C is 2.67 kPa. The net heat of combustion is 43.1 MJ/kg. The gross heat of combustion is 46.2 MJ/kg. The latent heat of fusion is $0.147 - 0.163$ kJ/g. The specific heat at $35 - 40°$ C (solid) is 2.604 kJ/kg K. The specific heat at $60 - 63°$ C (liquid) is 2.981 kJ/kg K. The thermal conductivity at room temperature is 0.23 W/m K. The average melted wax temperature around the base of the wick is $82 - 85°$ C. The maximum flame temperature is $1400°$ C [2].

For this study, small, paraffin wax votive candles were initially used, followed more extensively by tea lights. The motivation behind the study was to determine and predict, by physical property analysis, the effective burn

time of a single candle placed within a sealed container. Open environment candle studies are more prevalent than closed container studies, and tend to focus on, for example, soot creation, flame point study, heat flux study, heat rate versus time, and mass loss versus time [2][1]. Closed container studies are less useful for both manufacturers and fire investigators since, for a sealed container to have a prominent effect on a candle within it—such as self-extinguishing of the candle flame due to lack of oxygenated fuel or the build-up of spent product—the container must be sized relative to that of the candle. The larger the container, the longer the candle will burn before being extinguished, but the larger the container, the closer the study becomes to that of an open-container situation. A candle in a relatively-sized closed container is not necessarily useful for manufacturers and not traditionally significant to fire investigation.

As the study progressed, the paraffin wax candles were replaced with glass candles that contained a wick dipped into an ethanol mixture fuel. This replacement was made to better attempt to control the physical properties of the candle within the container, in an effort to understand the results of the study itself. The molecular formula for ethanol is C_2H_6O. The density is 0.789 g/cm^3. The melting point is $-114°$ C. The boiling point is $78°$ C. The vapor pressure at $20°$ C is 5.95 kPa. The viscosity at $20°$ C is 0.0012

Pa·s. The flash point is $13 - 14°$ C. The autoignition temperature is $362°$ C [9].

2. Fluid and Flame Dynamics

2.1. **The Navier-Stokes Equation.** A fluid at rest exhibits no shear stress and experiences isotropic pressure, meaning the pressure forces act in all directions with equal magnitude. For this simplified case, the force per unit mass that acts on the fluid as a result of pressure gradients and the weight of the fluid itself has a component in the x direction given by

$$f_1 = -\frac{1}{\rho}\frac{\partial p}{\partial x} - g\frac{\partial z}{\partial x},$$

where ρ is the density of the fluid, p is the isobaric pressure, and g is the acceleration due to gravity. If the fluid has viscosity, p is replaced with the pressure in the x direction, p_1. If the fluid is at the same time not at rest, we must allow for shear forces and we have

$$f_1 = \frac{1}{\rho}\left(-\frac{\partial p_1}{\partial x} + \frac{\partial s_3}{\partial y} + \frac{\partial s_2}{\partial z} - g\frac{\partial z}{\partial x}\right),$$

where s_2 and s_3 are the shear stresses in the y and z directions respectively. Allowing the fluid to be incompressible and Newtonian, meaning the fluid obeys linear relationships between shear stress and rate deformation, then

p_1 may be replaced with

$$p_1 - p + 2\eta \left(\frac{\partial u_2}{\partial y} + \frac{\partial u_3}{\partial z} \right),$$

with pressure p, fluid velocity u_i and viscosity constant η. At the same time, s_2 and s_3 may be replaced with permutations of

$$s_2 - \eta \left(\frac{\partial u_1}{\partial z} + \frac{\partial u_3}{\partial x} \right),$$

$$s_3 - \eta \left(\frac{\partial u_1}{\partial y} + \frac{\partial u_2}{\partial x} \right),$$

where $\eta \frac{\partial u_2}{\partial x}$, for example, is the magnitude of the shear stress normal to the x axis. As such, f_1 may be written in terms of the second derivatives of the fluid velocity,

$$f_1 - -\frac{\partial}{\partial x} \left(\frac{p}{\rho} + gz \right)$$
$$+ \frac{\eta}{\rho} \left(-2\frac{\partial^2 u_2}{\partial x \partial y} - 2\frac{\partial^2 u_3}{\partial x \partial z} + \frac{\partial^2 u_1}{\partial y^2} + \frac{\partial^2 u_2}{\partial y \partial x} + \frac{\partial^2 u_3}{\partial z \partial x} + \frac{\partial^2 u_1}{\partial z^2} \right)$$
$$- -\frac{\partial}{\partial x} \left(\frac{p}{\rho} + gz \right) - \frac{\eta}{\rho} \left\{ \frac{\partial}{\partial y} \left(\frac{\partial u_2}{\partial x} - \frac{\partial u_1}{\partial y} \right) - \frac{\partial}{\partial z} \left(\frac{\partial u_1}{\partial z} - \frac{\partial u_3}{\partial x} \right) \right\}.$$

The expression in curly brackets on the right-hand side of the equation is the x-component of the vector expression $\nabla \wedge \Omega$, where ∇ is the gradient and Ω is the local vorticity, the tendency of the fluid to "spin." However, by recognizing that similar expressions may be derived for the forces f_2 and f_3 in the y and z directions respectively, the total force per unit area acting

upon the fluid in vector form is

$$\mathbf{f} = -\nabla \left(\frac{p}{\rho} + gz \right) - \frac{\eta}{\rho} \nabla \wedge \Omega.$$

If we equate this force equation to the vector equation for the acceleration of a fluid,

$$\frac{D\mathbf{u}}{Dt} = \frac{\partial \mathbf{u}}{\partial t} + (\mathbf{u} \cdot \nabla) \mathbf{u},$$

where t is time, we have

(1) $$-\nabla p^* - \eta \nabla \wedge \Omega = \rho \frac{\partial \mathbf{u}}{\partial t} + \rho (\mathbf{u} \cdot \nabla) \mathbf{u},$$

where p^* is the excess mean pressure given by

$$p^* = \frac{1}{2} \rho \left(U^2 - u^2 \right),$$

for some uniform fluid velocity U [11].

Equation (1) is the "simplest" version of the *Navier-Stokes Equation*, which is the equation of motion for a fluid with viscosity and shear stress [11]. Outside of complex computer simulations, few exact analytical solutions are known for the Navier-Stokes equation. Analysis of Equation (1), however, can be done by making further simplifying assumptions [10]. For example, if $\mathbf{u} \cdot \nabla = 0$, the result may be used to study the low-speed gas flow approximations that occur in sealed compartment conditions, such as

those in this study [10][12]. As another example, the NIST Fire Dynamics Simulator (FDS) uses an approximate form of Equation (1) that filters out acoustic waves while at the same time allowing for large variations in density and temperature [12].

2.2. Flame Dynamics.

Both McGrattan et al. [12] and Liepmann et al. [10] give us the general governing equations of a Newtonian fluid, as illustrated in the NIST FDS.

We begin with Newton's Second Law for fluids, an equation for the conservation of momentum [12]. It is also a version of the Navier-Stokes equation as presented above [10].

$$(2) \qquad \frac{\partial}{\partial t}(\rho \mathbf{u}) + \nabla \cdot \rho \mathbf{u}\mathbf{u} + \nabla p - \rho g + \mathbf{f}_b + \nabla \cdot \tau_{ij}.$$

As above, ρ is the fluid density, $\mathbf{u}$ is the fluid velocity, p is the pressure, t is time, g is the acceleration due to gravity, and $\mathbf{f}_b$ represents external forces, as seen in the derivation of Equation (1) [12]. The term $\mathbf{u}\mathbf{u}$ is a diadic tensor of rank two, formed by juxtaposing pairs of vectors together with manipulation rules in line with the rules of matrix algebra [13]. Let $\mathbf{u} = [u, v, w,]^T$. Then the diadic is the tensor product of $\mathbf{u}$ and $\mathbf{u}^T$. Subsequently, applying the vector operator $\nabla = (\frac{\partial}{\partial x}, \frac{\partial}{\partial y}, \frac{\partial}{\partial z})$ to the tensor yields the term $\nabla \cdot \rho \mathbf{u}\mathbf{u}$. The

stress tensor, τ_{ij} is given by

$$\tau_{ij} = \mu \left(2s_{ij} - \frac{2}{3} \delta_{ij} \left(\nabla \cdot \mathbf{u} \right) \right),$$

$$\delta_{ij} = \begin{cases} 1 & i - j \\ 0 & i \neq j \end{cases}$$

with s_{ij} being the shear stresses given in the derivation of Equation (1) [12].

Conservation of mass is given in terms of density, ρ, by

$$(3) \qquad \frac{\partial \rho}{\partial t} + \nabla \cdot \rho \mathbf{u} = \dot{m}_{\beta}''',$$

where $\dot{m}_{\beta}''' - \sum_{\alpha} \dot{m}_{\beta,\alpha}'''$ is the production rate of gaseous species by evaporating particles. Equation (3) is found by taking the conservation of mass with mass fractions of individual gaseous species Y_{α},

$$\frac{\partial}{\partial t} \left(\rho Y_{\alpha} \right) + \nabla \cdot \rho Y_{\alpha} \mathbf{u} - \nabla \cdot D_{\alpha} \nabla Y_{\alpha} + \dot{m}_{\alpha}''' + \dot{m}_{\beta,\alpha}'''.$$

Summing across all gaseous species yields Equation (3) since $\sum Y_{\alpha} = 1$ and $\sum \dot{m}_{\alpha}''' - 0$ and, by definition, $\sum \dot{m}_{\beta,\alpha}''' - \dot{m}_{\beta}'''$. It is assumed, generally incorrectly, that the diffusion flux $\sum \nabla \cdot D_{\alpha} \nabla Y_{\alpha}$ is zero. This incorrect assumption is accounted for since transport equations are generally solved for total mass and all gas species save one, which implies that the diffusion coefficient for the chosen unsolved species is such that the sum is zero [12].

The equation for the transport of sensible enthalpy, the energy required to take the fluid from one temperature state to another, is given by

$$(4) \qquad \frac{\partial}{\partial t}(\rho h_s) + \nabla \cdot \rho h_s \mathbf{u} - \frac{Dp}{Dt} + \dot{q}''' - \dot{q}'''_\beta \nabla \cdot \dot{\mathbf{q}}'' + \varepsilon,$$

where the actual sensible enthalpy is given by $h_s - \sum_\alpha Y_\alpha h_{s,\alpha}$ with $h_{s,\alpha}$ a function of temperature, T, with specific heat, $c_{p,\alpha}$, [12],

$$h_{s,\alpha}(T) - \int_{T_0}^{T} c_{p,\alpha}(T')dT'.$$

The heat release rate per unit volume of a chemical reaction is given by $\dot{q}'''$, while $\dot{q}'''_\beta$ is the energy transferred to evaporating droplets. The conductive and radiative heat fluxes are given by $\dot{\mathbf{q}}''$,

$$\dot{\mathbf{q}}'' = -k\nabla T - \sum_\alpha h_{s,\alpha}\rho D_\alpha \nabla Y_\alpha + \dot{\mathbf{q}}''_r,$$

where k is the thermal conductivity, and $\dot{\mathbf{q}}''_r$ is the radiative term. The ε in Equation (4) is the dissipation rate, the rate at which kinetic energy is transferred to thermal energy due to viscosity,

$$\varepsilon \equiv \tau_{ij} \cdot \nabla \mathbf{u} - \mu \left(2s_{ij} \cdot s_{ij} - \frac{2}{3}(\nabla \cdot \mathbf{u})^2 \right),$$

where μ and s_{ij} are as above and τ_{ij} is the stress tensor also given above [12].

The equation of state for a perfect gas is given by

$$p = \frac{\rho \mathcal{R} \mathcal{T}}{\overline{W}},$$

(5)

where p is pressure, $\mathcal{R}$ is the ideal gas constant, $\mathcal{T}$ is the temperature, and $\overline{W}$ is the average volume [12].

As mentioned in the derivation of the Navier-Stokes equation, Equation (1), the divergence $\nabla \cdot \mathbf{u}$ may play a role in allowing for the study of low-speed gases. McGrattan et al. [12] note that the divergence term is found by taking the derivative along the path of velocity of the equation of state, Equation (5),

$$\nabla \cdot \mathbf{u} = \mathcal{D} + \mathcal{P}\frac{\partial \overline{p}_m}{\partial t},$$

where

$$\mathcal{P} = \frac{1}{\overline{p}_m}\left(\frac{\mathcal{R}}{\overline{W}c_p} - 1\right),$$

with $\overline{p}_m$ as the background pressure of the mth compartment or enclosure zone, and

$$\mathcal{D} = \frac{\dot{m}_\beta'''}{\rho}\frac{\overline{W}}{\overline{W}_\beta} + \frac{\overline{W}}{\rho}\sum_\alpha \nabla \cdot (\rho D_\alpha \nabla |Y_\alpha/W_\alpha|) + \frac{1}{\rho}\sum_\alpha \left(\frac{\overline{W}}{W_\alpha} - \frac{h_{s,\alpha}}{c_p T}\right)\dot{m}_\alpha'''$$

$$-\mathcal{P}w\rho_i y + \frac{\mathcal{R}}{\overline{W}c_p \overline{p}_i}\left[\dot{q}''' - \dot{q}_\beta''' - \nabla \dot{\mathbf{q}}'' - \sum_\alpha h_{s,\alpha}\nabla \cdot \rho D_\alpha \nabla Y_\alpha\right]$$

$$+\frac{\mathcal{R}}{\overline{W}c_p \overline{p}_i}\left[\dot{m}_\beta'''\sum_\alpha Y_{\beta,\alpha}c_{p,\alpha}\left(T_\beta - T\right) + \frac{\dot{m}_\beta'''}{2}|\mathbf{u}_\beta - \mathbf{u}|^2\right].$$

It should be noted that the pressure within the mth compartment zone is a linear combination of a background component and a flow-induced perturbation,

$$p(\mathbf{x}, t) = \overline{p}_m(z, t) + \tilde{p}(\mathbf{x}, t),$$

where $\overline{p}_m(z, t)$ is a function of the vertical background component and time t, and $\tilde{p}(\mathbf{x}, t)$ is the perturbation at location $\mathbf{x}$ at time t. For low-speed gas approximations, it can be assumed that temperature and density are inversely proportional, so the equation of state, Equation (5), for the mth pressure zone may be written as

$$\overline{p}_m = \rho \mathcal{T} \mathcal{R} \sum \left(\frac{Y_\alpha}{W_\alpha} \right) = \frac{\rho \mathcal{T} \mathcal{R}}{\overline{W}}.$$

Assuming a large enclosure or compartment fire, or a non-sealed compartment fire, $\overline{p}_m$ changes very little. In fact, the change in background pressure $\partial \overline{p}_m / \partial t$ is non-zero only if the compartment or enclosure is tightly sealed, as in the current study. Subsequently, in this study, $\overline{p}_m$ can not be considered a constant due to the decrease or increase of thermal energy and mass within the enclosure [12]. As such, let the time derivative of the mth pressure zone be Ω_m. In order to insure that a fire or flame lit within a sealed enclosure leads to an appropriate decrease in the divergence within the container, Ω_m is found by solving the divergence equation given above

for $\partial \overline{p}_m / \partial t$ and then integrating [12],

$$\frac{\partial \overline{p}}{\partial t} = \frac{\int_{\Omega_m} \mathcal{D} dV - \int_{\partial \Omega_m} \mathbf{u} \cdot d\mathbf{S}}{\int_{\Omega_m} \mathcal{P} dV}.$$

2.3. **Flame Phenomena.** As seen above, the governing equations of fire and combustion are complicated. Modeling fire behavior, which is needed to understand combustion physics as well as assist in fire prevention and investigation [14][12] is even further complicated by the conditions and environment of the fire itself.

Forest fires, for example, are affected by a number of factors, including available fuel, availability (or lack) of localized moisture, and the topography of the given terrain, as well as the ignition and cooling sequences of the individual fire [3]. Modeling and study of forest fires, by necessity, requires the modeling of roughly seven stages of combustion, namely preheating and pyrolysis, ignition, initial growth, secondary growth, flame decay, flame extinction, and cooling [3]. Despite this breakdown, modeling of forest fires is even further complicated by phenomena of fluid and fire dynamics that are independent of the above combustion phases. Fire whirls, for example, pose a rare, albeit catastrophic danger [4]. Fire whirls are cyclone-like phenomena where the fire is acted on by a source of angular momentum (wind, for example) which causes whirls to appear that are a wide variety of velocities and length scales [4]. Laboratory experiments of a 1.5-ft-high flame placed

within a 8-ft-diameter, 10-ft-high screen enclosure demonstrated that when the screen was rotated at merely 4 rpm, the flame grew to height of 15 feet, illustrating that even a gentle breeze generated by heated air can cause a heightened danger [4].

Enclosure fires, on the other hand, are equally, if not more so, complicated to model [14]. Often sub-models of turbulence, combustion, and radiative heat, whose strong interactions give rise to increasing complexity, are needed to model and study enclosed fires [14]. Despite the current adequacy of sub-models that deal with turbulence, thermal radiation, compressibility, and buoyancy, sub-models for turbulent combustion are lacking, since gasification and pyrolysis are difficult to model within an enclosure [14]. Added to this, physical interactions and phenomena are not necessarily understood within enclosure interaction. For example, the physical and chemical interactions between water spray and a fire plume are not fully understood, despite the wide use of water spraying sprinklers as fire suppressants and protection [15]. Furthermore, fluid dynamical effects, which do not inherently originate with combustion, may play a part in complicating the model or study of an enclosure fire. The *Coanda effect*, for example, is a tendency of a fluid moving with some velocity to be attracted towards or curl around a nearby surface; an example is seen when liquid is being poured from a vessel and the liquid curls around the rim despite being

poured, dripping along the edge [11]. Despite being discussed as early as 1800 [16] and being discovered as an application in 1910 [16] the Coanda effect played an unexpected role in the 1987 King's Cross fire, which resulted in the deaths of 31 people [17]. The Coanda effect combined with a flashover effect commonly found in fire dynamics (where nearby material is superheated in the presence of a nearby flame that it is not in direct contact with, promptly igniting) to form a *trench effect* whereby flames laid down below the walls of an escalator, remaining unseen by fire fighters adjacent to the escalator until the flashover effect caused the fire to spew from the mouth of the escalator, causing major damage [17][18].

2.4. **Oxygen Level at Flame Extinction.** The National Institute of Standards and Technology notes "a diffusion flame immersed in a vitiated atmosphere will extinguish before consuming all the available oxygen from the atmosphere" [12]. For use within the NIST Fire Dynamics Simulator (FDS), studies on small controlled-volume environments were conducted. Within the control volume with a bulk temperature T_m, a mass m, and an average specific heat $\overline{c_p}$, complete combustion of the oxygen contained therein would release energy given by

$$Q - mY_{O_2}\left(\frac{\Delta H}{r_{O_2}}\right),$$

where Y_{O_2} is the oxygen mass fraction and $\Delta H/r_{O_2}$ has a constant value of approximately 13100 kJ/kg for most fuels of interest. For adiabatic conditions, the bulk temperature of the gases within the control volume would be raised by the energy released due to the combustion of the available oxygen. This is demonstrated by

$$Q - m\overline{c_p}(T_f - T_m),$$

where T_f is the final temperature after flame extinction, and $\overline{c_p}$ can be calculated based upon the composition of the combustion products,

$$\overline{c_p} - \frac{1}{T_f - T_m} \sum_{\alpha} \int_{T_m}^{T_f} c_{p,\alpha}(T)dt.$$

For the studies used within the FDS, the combustion products are assumed have an average specific heat of 1.2 kJ/kg/K for the temperature range of interest in order to simplify the analysis. This value is similar to the specific heat of nitrogen, the primary component of the combustion products themselves [12].

By equating both of the above equations for Q, the relationship between the oxygen mass fraction and the adiabatic temperature rise within the control volume can be evaluated. As such,

$$Y_{O_2} - \frac{\overline{c_p}(T_f - T_m)}{\frac{\Delta H}{r_{O_2}}}.$$

Letting the critical adiabatic flame temperature have a constant value of approximately 1700 K for typical hydrocarbon diffusion flames, the relationship between the limiting oxygen mass fraction—the mass fraction of extinction—and the bulk temperature T_m of the control volume is

$$Y_{O_2,\text{lim}} = \frac{\overline{c_p}(T_{f,\text{lim}} - T_m)}{\frac{\Delta H}{r_{O_2}}} \approx \frac{1.2(1700 - T_m)}{13100}.$$

For a control volume near room temperature, i.e., approximately 300 K, the limiting oxygen mass fraction would be given by

$$Y_{O_2,\text{lim}} = 0.128,$$

which is consistent with experiments that measured the oxygen concentration at extinction, finding them to be 12.4% to 14.3% . As such, the FDS is hard-coded with a default value of 15% for the oxygen level at flame extinction within a control environment [12].

3. Methods

The motivation for this project was to generate a model that would predict the burn time before extinction of a candle placed within a sealed container, based upon container volume and type of candle. Initially, to determine the basic feasibility of the proposed project, a single paraffin tea light was placed inside an upturned cylindrical glass vase, with vase sizes ranging from 700 ml to 1200 ml. The candle was placed on a small, raised

platform within a metal cooking sheet, with a layer of water lining the sheet to a depth of roughly one centimeter. The glass vase was placed open-side down over the burning candle, the edge of the opening of the vase beneath the surface of the water, effectively sealing the interior of the vase from the surrounding air. Time measurements were taken to determine rough extinguishing times for the candle flame under the various vase sizes.

Paraffin tea lights were then placed on inverted 200 ml glass beakers within two glass fish aquariums, one 5 gallon ($40.0\text{cm}\times20.4\text{cm}\times23.3\text{cm}$), one 10 gallon ($50.1\text{cm}\times29.8\text{cm}\times27.5\text{cm}$). The aquariums were placed open-end down into a plastic tub ($56.4\text{cm}\times37.8\text{cm}\times15.5\text{ cm}$) filled with water to a height of 2.5cm, once again forming airtight conditions within the respective aquariums. The mass of each paraffin tea light was recorded twice, once prior to ignition and again after flame extinction, to determine mass-loss during combustion. Time measurements were taken until flame self-extinguishing, and broad-spectrum Pasco light sensors (PS-2150, spectral response 300 nm to 10000 nm) were used in an attempt to determine exact point of flame extinction. The light sensors were placed outside the given aquarium, initially directly above the flame location, several centimeters above the glass, and then in a lateral position, aimed at the flame location through the side of the aquarium. A layer of water 1 cm in depth was placed

atop the inverted aquarium to ensure that the glass did not fracture due to heat during the experiment.

A plexiglass container (35.7cm×27.6cm×27.5cm) was then designed and built to allow for greater control of the ignition of the candle with regard to initial oxygen levels within the container the use of the inverted aquariums required that the time between candle ignition and the placement of the inverted aquarium over the candle, into the water, creating the seal, was non-trivial. A hole (12.0 mm diameter) was drilled within one of the sides of the container, the hole just large enough to allow the passage of the nozzle of a butane lighter (10.0 mm diameter), which would ignite the candle after the container was sealed, the lighter then being removed and the hole quickly sealed with masking tape. An ethanol mix candle (200 ml) was placed within the container, in the center of the bottom plexiglass plate, 8.5 cm from the from the front wall. A Pasco oxygen sensor (PS-2126) was then placed within the container, within one of the various grid locations located on the side of the container. The location of the sensor varied per test run. A Pasco light sensor (PS-2150) was affixed above the top of the container, directly in line with the candle location, aimed downwards (*see Figure 1 and Appendix: Figures 28 and 29*).

A wax ring (1.1 cm thickness) was poured around the edge of the top plate of the container, and water (1.0 cm depth) was placed within the
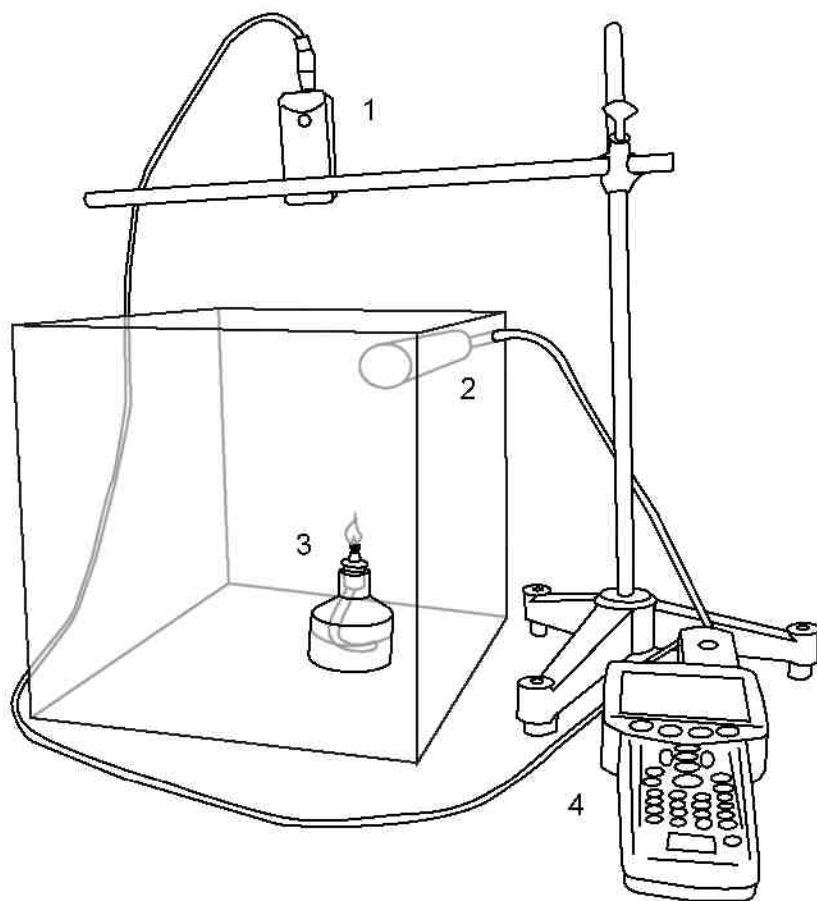
FIGURE 1. Experimental apparatus. 1: Light sensor (PS-2150). 2: O_2 sensor (PS-2126). 3: Ethanol candle. 4: Data-logger (PS-2002).

wax ring in an effort to keep the top panel from fracturing due to heat during the experiment. Between each run of the experiment, the plexiglass walls were wiped down to remove excess condensation and a delay time of

20 minutes was allowed for the return of the atmosphere within the now-opened enclosure to return to atmospheric baseline.

Further testing was done with the mass loss rate of paraffin wax tea lights, as tea lights were placed upon a scale and burned, both in open air and within the closed, plexiglas container.

The ethanol candle was then placed within the enclosed container, atop a wooden block measuring 127mm×86mm×37mm. By rotating the block along its sides for each experiment, candle heights of 37mm, 86mm, and 127mm were achieved. For each height placement, the ethanol mass loss was measured against burn time, with a control run where the candle was placed alongside the block within the enclosure, the candle at 0mm height.

The distance the ethanol within a given candle had to travel up the wick to reach the ignition point was measured by fixing the length of the wick and varying the height of the ethanol. Mass loss for a fixed burn time was then recorded for each ethanol height.

Finally, the shape of the tip of the wick was studied during combustion. The three shapes studied were the control shape the unmodified wick an equilateral triangular-shaped tip, and a flat, rectangular-shaped wick. Two sets of experiments were run with each shape, each with a five minute burn time. The second run involved lengthening the control wick by 1cm,

lengthening the triangular wick by 1.5cm, and lengthening the rectangular wick by 2cm.

A computer simulation (*see Appendix: Code*) was written using the C programming language. The simulation attempted to predict the approximate oxygen loss per 2-dimensional gridded region within the test container, based upon flame location, convection and diffusion.

4. RESULTS

The initial series of experiments conducted with an ethanol candle enclosed within the plexiglass container yielded results that were not initially unexpected (*See: Figure 2 and Appendix*).

For example, flame extinction happened at 336 seconds with an oxygen level of 15.0, at 345.5 seconds with an oxygen count 15.2, at 351 seconds with an oxygen count 14.7, and at 361.5 seconds with an oxygen count 14.9.

However, the second series of experiments, produced results that varied substantially (*See: Figure 3 and Appendix*).

For example, in one experiment, the ethanol candle extinguished at 405 seconds with an oxygen count 16.0, yet another extinguished at 210 seconds with an oxygen count 17.5, and another extinguished at 150 seconds with an oxygen count 18.3. Still other experimental runs included flame extinction at 360 seconds with an oxygen count 16.4 followed by a run with extinction
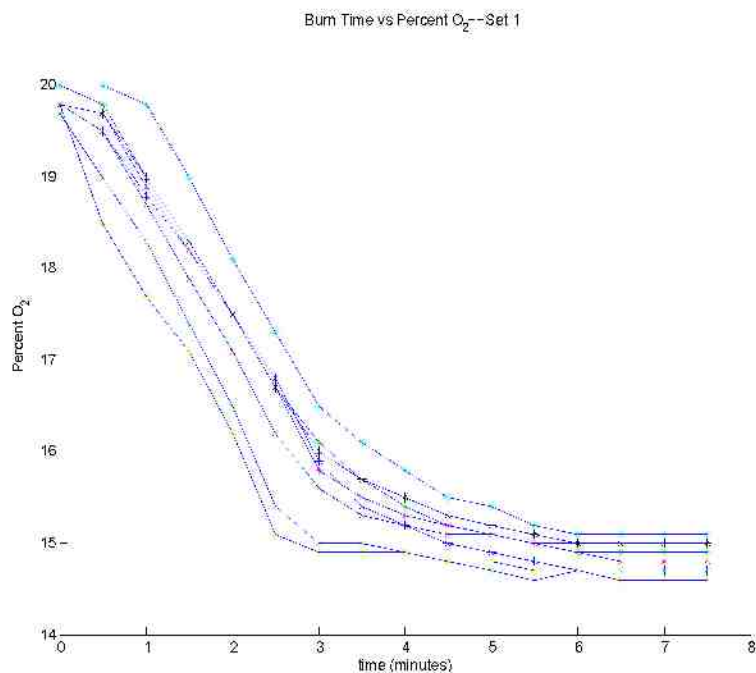
Burn Time vs Percent O$_2$--Set 1

FIGURE 2. Final percent O$_2$ versus burn time: Series 1. Data point types vary depending on placement of oxygen sensor. Flat lines at end of curve indicate burn out.

at 210 seconds with an oxygen count 17.0; followed by a run with extinction at 330 seconds with an oxygen count 15.9, followed by a run with extinction at 150 seconds with an oxygen count of 16.5.

In order to assess the variation in flame extinction times and final oxygen levels, mass loss versus burn time data was collected for both ethanol candles and paraffin wax tea lights (*See Figures 4, 5, 6, and 7*).

The ethanol level within a candle was measured along with initial and final masses, and burn times in open air. Two runs were made with an
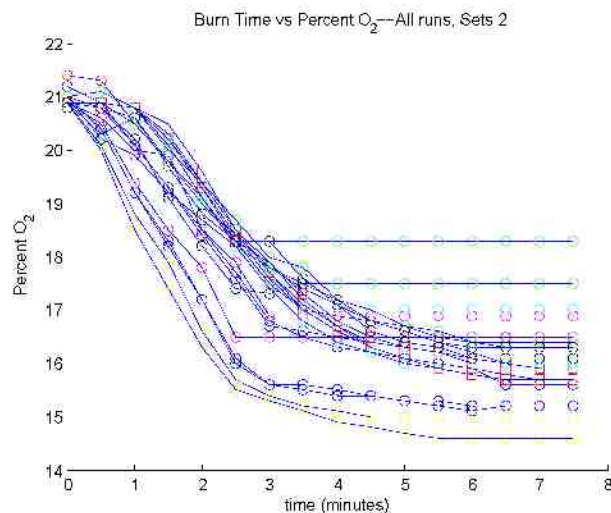
FIGURE 3. Final percent O_2 versus burn time: Series 2. Data point types vary depending on placement of oxygen sensor. Flat lines at end of curve indicate burn out.

initial ethanol level of 30 mm. For the first of these runs, the initial mass of the ethanol was 225.6 grams and the final mass was 223.5 grams after 5 minutes, for a mass difference of 2.1 grams. For the second run, the initial mass of the ethanol was 223.4 grams and the final mass was 221.3 grams after 5 minutes, for a mass difference of 2.1 grams. A third and fourth run were made with the initial ethanol level of 22 mm. The third run had an initial ethanol mass of 206.5 grams and a final mass of 204.6 grams after 5 minutes, for a mass difference of 1.9 grams. The fourth run had an initial
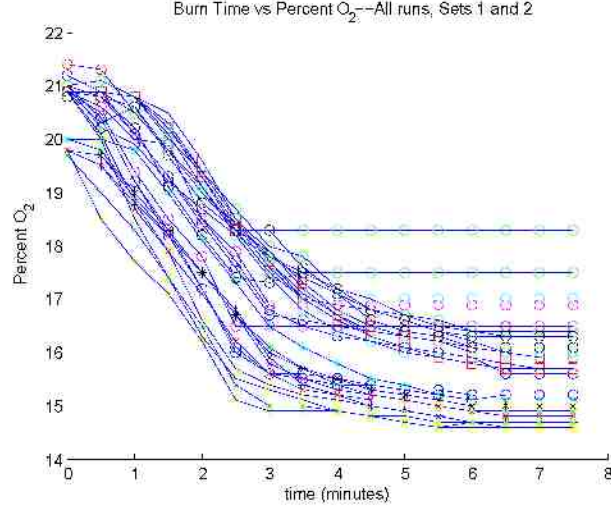
FIGURE 4. Final percent O_2 versus burn time: Series 1 and 2. Data point types vary depending on placement of oxygen sensor. Flat lines at end of curve indicate burn out.

ethanol mass of 204.5 grams and a final mass of 202.8 grams after 5 minutes, for a mass difference of 1.7 grams.

The height of the ethanol candle within the enclosed container was studied. For the control test, with the candle at 0mm height, placed next to the block inside the container, the initial ethanol mass was 198.5 grams, and the final mass was 197.4 grams, for a mass loss of 1.1 grams, with a burn time before extinction of 6 minutes, 26 seconds. For $h = 37$mm, the initial ethanol mass was 197.4 grams, and the final mass was 196.2 grams,
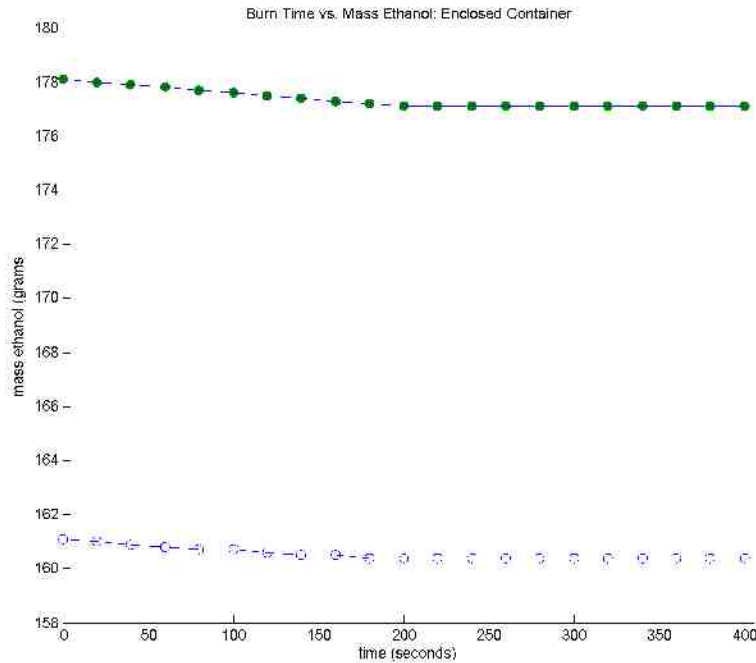
FIGURE 5. Mass Loss versus burn time of ethanol candle, enclosed. Two runs with separate initial masses.

for a mass difference of 1.2 grams, with a burn time before extinction of 5 minutes, 55 seconds. For $h = 86$mm, the initial ethanol mass was 196.2 grams, and the final mass was 195.0 grams, for a mass loss of 1.2 grams, with a burn time before extinction of 5 minutes, 29 seconds. Finally, for h 127mm, the initial ethanol mass was 196.0 grams, and the final mass was 194.8 grams, for a mass loss of 1.2 grams, with a burn time before extinction of 3 minutes, 30 seconds. It should be noted that the aforementioned wax ring and water layer were added to the glass top of the enclosure for the $h = 127$mm height experiment to protect the glass.

29
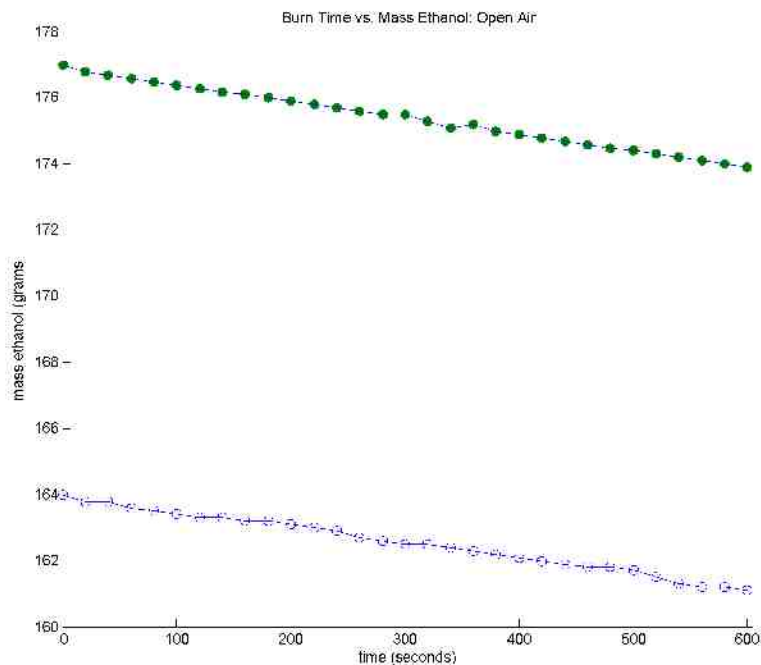
FIGURE 6. Mass Loss versus burn time of ethanol candle, open air. Two runs with separate initial masses.

Finally, the shape of the tip of the wick of an ethanol candle was studied, to determine its affect on combustion. For the control wick—meaning an unmodified wick—the initial mass of ethanol was 183.1 grams and the final mass was 181.6 grams, for a mass difference of 1.5 grams. Next, the tip of the wick was cut into a triangle shape. The initial ethanol mass was 179.2 grams and the final mass was 177.7 grams, for a mass difference of 1.5 grams. Finally, the tip of the wick was cut into a shallow rectangle, the width greater than the height. The initial ethanol mass was 182.3 grams and the final mass was 180.8 grams, for a mass difference of 1.5 grams.
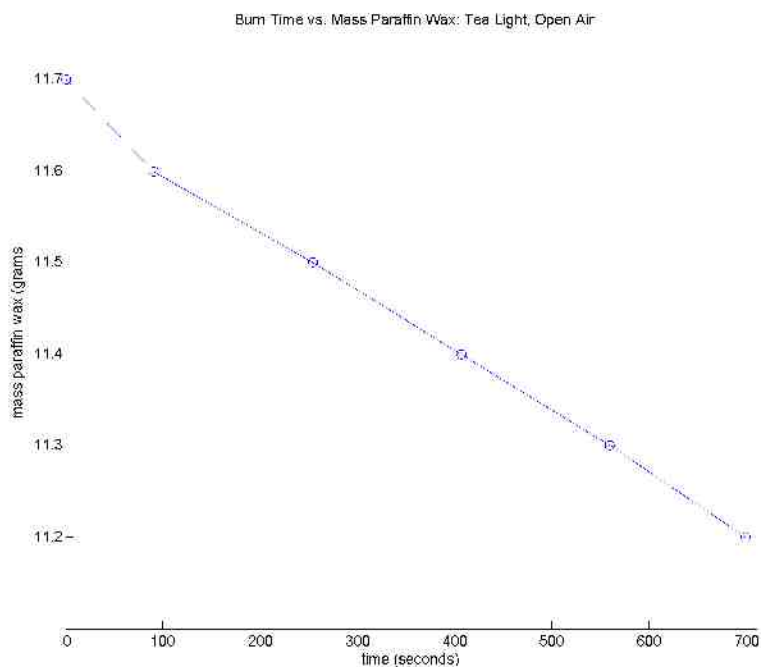
FIGURE 7. Mass Loss versus burn time of paraffin wax tea light, open air.

The wick shape experiment was re-conducted with length added to the different shaped wicks. The control, unmodified wick was lengthened by 1 cm. The initial ethanol mass was 181.5 grams and the final mass was 179.8 grams, for a mass difference of 1.7 grams. The triangular cut wick was lengthened by 1.5 cm. The initial ethanol mass was 177.5 grams and the final mass was 175.6 grams, for a mass difference of 1.9 grams. Finally, the rectangular—flat cut—wick was lengthened by 2 cm. The initial ethanol mass was 182.4 grams and the final mass was 180.2 grams, for a mass difference of 2.2 grams. It should be noted that the height of the flame itself
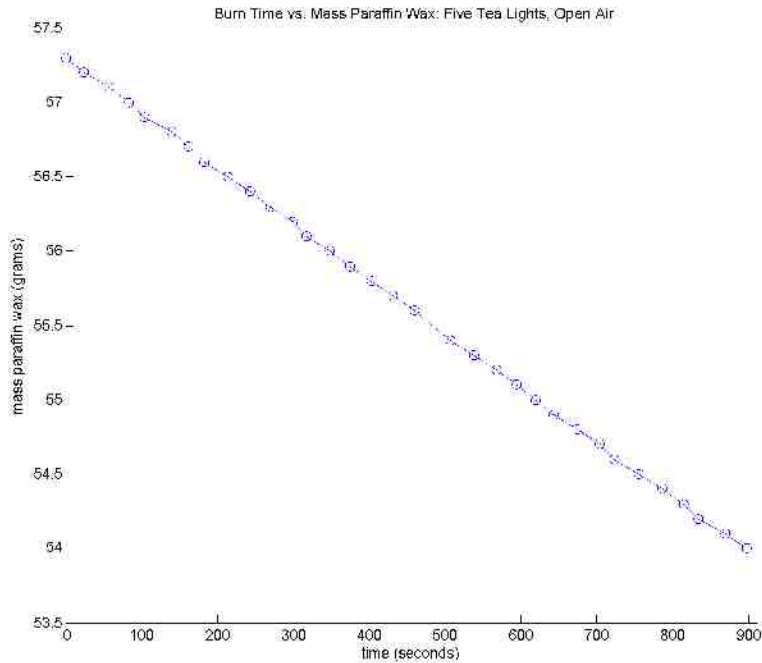
FIGURE 8. Mass Loss versus burn time of five paraffin wax
tea lights burned and weighed simultaneously, open air.

was higher in the wick-lengthened tests than in the above, non-lengthened
tests.

5. ANALYSIS

For initial runs of our project, the oxygen level at flame extinction ap-
proached the NIST FDS target number, given in Section 2.4, within error
bars (*Figure 2*). However, subsequent test runs not only failed to reproduce
the data of the initial runs, but also failed to approach the FDS target of
15% with any constancy (*Figure 3, Figure 4*).
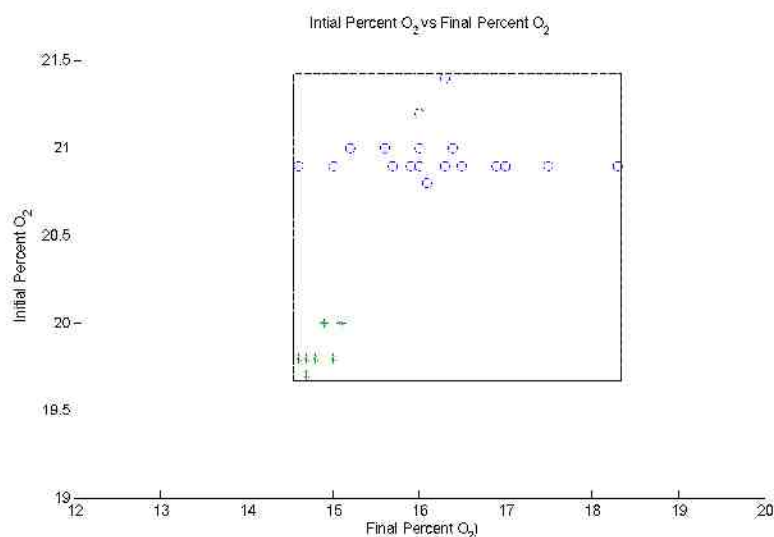
FIGURE 9. Final percent O_2 versus initial percent O_2. Boxed region indicates experimentally determined limits.

Various secondary experiments were performed to attempt to isolate any previous experimental errors. For example, varying the height of the ethanol candle above the bottom of the container resulted in the same mass loss per burn, although the candle burned out quicker at greater heights. Added to this, the length of the wick, not unsurprisingly, varied the length of flame, regardless of burn time. It seems likely that the faster burn time with an elevated candle could be attributed to the fact that there should be less of the bulk oxygen in the container above the candle, and that the action of combustion did not draw enough of the unspent oxygen from below the candle upwards to keep the flame burning. However, there were runs where
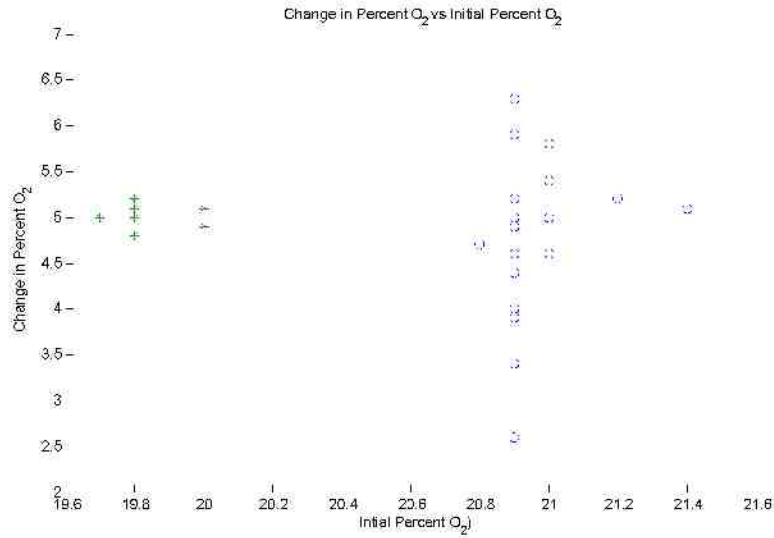
FIGURE 10. Change in percent O_2 versus initial percent O_2.

the candle was placed on the bottom of the container, with a subsequent smaller burn-out time (150 seconds, for example, with an oxygen percentage of 18.3 to 210 seconds with a oxygen percentage of 17.5—*see Appendix: Figure 17*).

In light of this, another experiment was conducted using a different ethanol candle, still located in the center of the bottom of the enclosure, while the oxygen sensor was located in the same location that generated the 150 seconds, 18.3 O_2% and the 210 seconds, 17.5 O_2% (namely, 0cm right of the center, 20cm above the bottom). The result, however ran from a burn time of 390 seconds with a final percent O_2 of 16.4, to 210 seconds with 17.0 percent O_2, to 330 seconds with 15.9 percent O_2, to 150 seconds

with 16.5 percent O_2. Concerned at this point that the ethanol within the two previous candles had in some way been compromised, a third candle was filled with new, pure ethanol and placed again at the center of the bottom of the enclosure, the oxygen sensor location unchanged. The result was a burn time of 180 seconds with a resulting percent O_2 of 16.9, which again, seemed closer to the newer results than those results that initially approached the NIST figures.

Added to this, experiments were conducted in open air and within the enclosed container where the ethanol candle was placed on a scale and allowed to burn, the mass loss recorded, and, in the case of measuring mass loss within the enclosed environment, the percent oxygen was also measured. The chemical equation of combustion for ethanol is given by

$$C_2H_6O + 3O_2 \rightarrow 2CO_2 + 3H_2O.$$
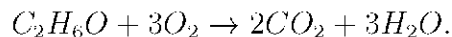
Analysis of this equation in comparison with the resulting mass and oxygen loss both inside and outside of the enclosed container agree well together, indicating that the ethanol was pure and burning well (*see Figures 5 and 6*).

It should be noted that when the varying candle elevation experiments initially resulted in the cracking of the glass container top due to the proximity of the flame itself. A new lid was affixed and a wax ring was poured

around the edge of the top, allowing a layer of water to be placed on the top of the container to keep the glass of the top from over-heating. However, this occurred early in the varying height experiments, the results of which are discussed above. As such, a new glass top was affixed to the container and the experiment, with a candle burning new, pure ethanol, was placed once again at the center of the bottom, the oxygen sensor 9cm right of center, 20cm above the bottom. The result was a burn time of 480 seconds with a final percent O_2 of 15.3—much closer to the NIST target. The previous, wax-ringed lid was replaced on the container and the experiment, with new, pure ethanol—the candle at the center of the bottom, the O_2 sensor at 9cm right of center, 20cm above the bottom—was re-conducted. In this case, the flame extinguished at 180 seconds with a final percent O_2 of 16.3. Once more re-conducting the experiment with the wax-ring lid, the percent O_2 went from an initial value of 20.9 to a final value of 16.4. Switching lids once more to the new, non-wax-ringed lid, the percent O_2 went from an initial value of 20.8 to 15.4. In each of these cases, it should be noted that with the wax-ringed lid, the initial bulk temperature within the container ranged from an initial value of 24° C (for two back-to-back experiments) to a final temperature of 30.5° C and 27.4° C for the back-to-back experiments respectively. On the other hand, two back-to-back experiments with

the new, non-wax-ringed glass top resulted in initial temperatures of 23.6°C and 26.9°C respectively, and final bulk temperatures of 27.9°C and 23.1° C.

These results suggest that the wax-ring might actually be interfering with the experiment. However, another round of experiments using the new glass, no-wax-ringed top were conducted with an ethanol candle containing new, pure ethanol and placed in the same location as the previous set of experiments—candle at bottom center, sensor at 9cm right of center, 20cm above bottom. To keep the glass top from overheating, the glass was moistened prior to flame ignition. Flame extinction occurred at 211 seconds with a final percent O_2 of 16.3, a result similar to that found using the wax-ringed lid. Similar results were then found when using a completely dry top: flame extinction at 174 seconds, with a final percent O_2 of 16.7. Further experimental runs were conducted, some where the walls of the container were wiped down with a moist sponge, others with the wax-ringed top in place and the walls of the container moistened (*see Appendix: Figure 22*).

Initial analysis of the NIST governing equations for the bulk control volume given above suggest that the bulk temperature was raised and more energy released—by the candle due the specific heat of the system changing with the inclusion of the wax and water layer on the top of the container. However, while this might result in a faster burn time since the oxygen mass fraction Y_{O_2} would increase, this should not necessarily imply that the final

percent O_2 would be any different simply because that final percentage was reached more quickly. Moreover, despite initial results with the new glass, non-wax-ringed lid being closer to NIST standards, subsequent experimental runs with the same lid yielded results similar to that of the wax-ringed lid. If indeed the wax and water layer on the wax-ringed lid raised the specific heat of the system and if, indeed, the resulting O_2 percentages were a result of this specific heat increase then the results with the non-wax-ringed lid, which would presumably have a lower specific heat, should closer match the NIST standards on multiple runs, which they do not. Added to this, it can be seen that there is no striking difference between having no wax and water layer and having a wax and water layer indeed between wiping and not wiping down the container walls between each run—at all (see *Appendix: Figure 24*).

Subsequent analysis of the computer simulation designed for this project (see *Appendix: Code*) revealed that, despite being only a two-dimensional model of the three-dimensional closed container system, that the target percent O_2 of the NIST standard was reached with only a bi-directional diffusion term included in the code. Despite that fact that certain variables were hard-coded within the program based upon approximate values, the results of each run approached 15% with each run. (see *Appendix: Code*

Output). Oddly, then, it was the experimental data, rather than the calculated data, that deviated time and again.

The question, then, is why are the experimental results deviant? A question could be raised about the accuracy of the Pasco oxygen sensor, but regardless of whether the sensor was functioning properly, or regardless of whether the data-collector had, for example, been zeroed properly, the deviation in combustion times would indicate a problem other than faulty data collection. Along those lines, the container itself was checked time and again for leaks, and the silicon seals were reinforced on at least one occasion. Although there were experimental runs where one of the small holes in the side of the container was not properly sealed, this oversight seemed to have no overall effect on the total results, which seemed to deviate from each other regardless of whether a hole was not properly sealed. Added to this, the measured burn times before flame extinction varied widely (*see Appendix: Figures 25 and 26*) indicating that, even if there were problems with the sensing equipment, these problems alone would not account for the deviant results.

The complexity of the above NIST equations for Q, $\overline{c_p}$, and Y_{O_2} in a sealed environment alone, not including the complexity of the governing fluid dynamical and flame dynamical equations given in Section 2, might reveal the source for the deviant experimental results. However, it is difficult

to determine which, if not all, of the governing equations might contribute a term or a whole that would explain the variation in both burn time and final percent O_2 regardless of experimental setup.

The primary transport phenomena for the gaseous species within the sealed container are diffusion and convection [4][12]. In some cases, for example, combustion can drive convection through the buoyant properties of the gaseous species present [4]. In large scale models, and in actual recorded fires, this convection-buoyancy phenomena can lead to dramatic fire whirls. Under the auspices of the Boussinesq model, the density of a given set of gaseous species is replaced by an ambient density ρ_0 in the conservation of momentum equation (2) with an assumption that the density variations within the set of gaseous species is small [4]. As such, the Boussinesq approximation for the fluid head which relates the energy of a fluid to the height of an equivalent static column of said fluid—is given by

$$\mathcal{H} \equiv \frac{p - p_0}{\rho_0} + \frac{1}{2}|\mathbf{u}|^2 + gx,$$

where p is the dynamic pressure, p_0 is the ambient pressure, $\mathbf{u}$ is the total velocity, and g is the acceleration due to gravity [4] [5]. Experiments on large scale flames (acetone flames of an initial height of 1.5 feet contained within a 4-in diameter can which was placed within the center of 10-ft-high, 8-ft-diameter wire screen that was rotated 4 revolutions per minute) revealed

that the flames, during the 4 rpm screen rotation, reached a height of 15 ft [4]. Granted, there was no rotational component added to the ethanol candle or to the sealed container itself during our experiments, however, it might be possible that the ethanol flame within the sealed environment created a diffusion process that caused a convection through buoyancy not unlike that seen in the formation of fire whirls. If this was the case, then the dynamic transport of both spent product and unused gaseous species fuel in the container might develop randomized patterns rather than a more predictable circulation of gases that would feed the flame and transport spent product away. Further complicating this, such a relatively small enclosed environment might have unknown initial conditions that are more sensitive than otherwise, meaning that any minor shift in the environment—perhaps due to the minor differences made by inserting and removing the lighter could add further randomized behavior to the system in the form of buoyant circulation. However, since it would be virtually impossible to account for this randomized, buoyant circulation without further testing, or without further developing a more complicated computer simulation, there is no way to determine if this effect was indeed present and, if so, whether the effect caused a seemingly randomized transport of gaseous fuel and spent product that worked to vary the percent oxygen near the sensor with each run.

Hamins et al, however, note that, in their studies of paraffin wax candles, it took from 12 to 15 minutes to achieve steady burning behavior, after which there was little change in, for example, the mass loss rate of the candle. The experimental apparatus described in these experiments was not a sealed container, and the wax candles in question were allowed to burn for upwards of 130 minutes without self extinction due to loss of oxygen [2]. However, under the sealed container conditions of our experimental runs, the burn time did not exceed 7 minutes without flame extinction. This means that in each of our experiments within the sealed container, the ethanol flame burned out before reaching what might have been a steady burn rate. Granted, the studies mentioned by Hamins et al. were with paraffin wax candles and not ethanol candles, but it begs the question as to whether this distinction is irrelevant. In the wax candle experiments, once the steady combustion was reached there was little reported change in any of the experimental results. If the lower bound for steady burning behavior of ethanol candles is beyond that which could be reached before flame extinction, then it is possible that the lack of steady combustion might in some way effect the experimental results due to the propensity of more random diffusion and convection within the combustion process. For example, in measuring the mass loss rate of the wax candles, Hamins et al. found that there was a steady, rapid increase within the first 10

minutes of combustion before the mass loss rate tended to level off after the 12 to 15 minute approach of steady burn behavior, with the mean mass loss rate reported to be 0.105 g/min. Added to this, the flame heights after ignition of paraffin wax candles also reach a steady trend after the 12 minute mark. On the other hand, it took roughly 5 minutes less to reach steady state with pre-burned paraffin wax candles, which was surmised to be due to the pre-existing formation of a wax "cup" at the base of the wick [2]. Again, this might indicate that for ethanol candles in the sealed container, the flames themselves were not allowed to reach a steady state, burning out long before that steady state could be reached, possibly resulting in more variable combustion behavior, in turn resulting in highly variable final percent oxygen levels despite flame extinction. Burning both the paraffin wax tea candles and the ethanol candles outside of the enclosed environment, for example, resulted in repeatable mass loss data that seemed to match that of published experimental studies (*see Figures 5, 6, 7, and 8*) which seems to support this hypothesis [2].

Since the flames of the ethanol candles in the sealed container may not have reached steady burn behavior, it is possible that, prior to extinction and long before steady burn behavior could appear, the turbulent structure of the buoyant flames themselves—the fire plume—might have contributed to an inconsistent gaseous species and spent product distribution [19][1].

Researchers measured terms appearing in the momentum equation, Equation (2), and the mean energy equation, Equation (4). Within the auspices of turbulent, buoyant flames, the researchers noted axial velocity fluctuations u'/u_0 and intensities of temperature fluctuations $T'/\Delta T_0$, indicating that prior to the onset of steady combustion behavior, there are fluctuations in relative velocity of the flame itself, as well as fluctuations in flame temperature and bulk temperature close to the flame source [19]. Rapid fluctuations due to small turbulence caused by the rapidly varying flame prior to steady combustion, might cause not only unsteady percent oxygen readings but also might cause the flame to self-extinguish under the rapid fluctuations of its own momentum [19].

Considering that enclosed environment flames have been studied, and conclusions reached for larger scale containments (*see Section 2.4*) it is possible that the enclosed environment itself—especially of such small scale relative to the candle—may have contributed to the non-repeatability of the experiment by confining both the gaseous fuel and spent product in such a way that no consistent percent oxygen results could be obtained, while at the same time varying the burn time to such an extent. As diffusion and convection, under the turbulent, buoyant conditions existing prior to steady flame behavior, varied after ignition due to the constraints of the container itself, it is possible that flame extinction occurred even at high levels of

percent O_2 due to the fact that the spent product that would normally be carried away from the flame may not have been properly transported, resulting in premature flame asphyxiation as if the flame were located in a second, localized "enclosed" container, the boundaries of which were the turbulent flows themselves. Similarly, the sealed conditions might have resulted in a heightened turbulence immediately after flame ignition that might have snuffed the flame by its own initial momentum. This, however seems less likely than that of an uneven propagation of both gaseous fuel and spent product due to rapid fluctuations prior to steady flame behavior.

6. Conclusions

Initially, with the use of paraffin wax votive and tea light candles placed within enclosed, glass containers, the burn time before flame extinction and oxygen levels of each candle were collected with the purpose of creating a model for determining the total burn time and final percent oxygen of any given type and size of candle, and any volume of enclosed environment. Eventually, a closed, plexiglass container was manufactured, and ethanol-mix candles were used, and again the burn time before flame extinction and the final percent oxygen were measured. However, as the data shows, the experiment was non-repeatable and no immediately useable pattern was discovered.

It remains, at this stage, uncertain as to why the experiment is non-repeatable, especially in light of previously cited studies which generated final percent oxygen levels that were on par with calculation [12]. The complexity of the governing equations of both fluids and combustion may give a clue as to the inability to measure consistent data. It is possible that the diffusion and convection dynamics within the environment led to the non-repeatability with small-scale versions of the large-scale Boussinesq model of fire whirls, leading to flame extinctions that were not directly the result of low oxygen percentages.

Since, in each run of the experiment, flame self-extinction happened before the combustion process could reach equilibrium, it is possible that the flame dynamics within our process were not stable enough to be repeatable [2]. It is possible that in the period between ignition and flame extinction, since the combustion process was not in equilibrium, that varying burn rates, flame height, flame and ambient temperatures, and pressures could generate a turbulent environment. This environment might not only extinguish the flame outright, but lead to chaotic behavior of gaseous species fuel and spent product, in turn leading to a randomized dynamic environment. Since the final percent oxygen measured is that of the entire enclosed container, it is possible that the non-equilibrium stage of flame dynamics created a smaller, more localized environment around the flame

itself, wherein fresh gaseous species fuel and spent product were essentially isolated from the greater whole of rest of the environment within the container. In this way, it may be possible that the non-equilibrium dynamics themselves helped to create a second, variable "enclosed" condition immediately around the flame, causing flame extinction at varying times and varying *overall* final percent oxygen.

At this stage, it can be said that, with such a low-cost experimental set-up, there is no simple way to adjust the experiment to get repeatable results. It is possible, then, that in future experiments, better materials or more uniform construction may be used in creating the experimental enclosed environment. It is also possible that more accurate measuring equipment may be used, although, as was noted, the varying burn times before flame self-extinction indicate that the final percent oxygen measurement equipment was neither faulty or completely inaccurate. The introduction of a small, motorized fan within the enclosed container might be used to force a more dynamic, turbulent flow that did not result directly from non-equilibrium flame dynamics. By necessity, the inclusion of a fan would complicate the fluid dynamic process, but it might lead to more repeatable results. If the fan were moved from location to location within the container, and the experiment repeated, the data gleaned might help understand the diffusion and convection process present, perhaps allowing for better overall data

collection, since the fan would force a possible equilibrium condition in the container itself by forcing gaseous species fuel and spent product to move under the auspices of something other than combustion process itself. However, the modeling process would be greatly complicated with the inclusion of the fan, but this might be an unavoidable necessity, given the complexity of the fluid dynamical governing equations to begin with.

Further, it might be possible to establish an experimental environment wherein the ignition system is entirely contained within the enclosed container with the candle. Although this would necessitate a greater level of funding, including a remote ignition system would allow for fewer changes in any unknown, sensitive initial conditions. For example, the current experimental set-up has a small hole drilled into one wall of the container to allow for the introduction and removal of a lighter. Without this hole, however, it would have been necessary to open the container lid, light the candle, and then close the lid, potentially changing the initial conditions within the container even more dramatically than simply introducing and removing the lighter through the small hole. It should be noted that initial attempts to use a remote ignition system were attempted early in the experiment, but were abandoned due to difficulty and expense.

A three-dimensional computer model might also be implemented, however, it should be noted that the two-dimensional computer simulation that

was created did not display any of the non-repeatability that was found in the lab. Before implementation of the three-dimensional model, then, it might be more prudent to re-work the two-dimensional model to see if the experimenters could force the model to return non-repeatable results. This could then give a clue as to how to implement a three-dimensional model by enumerating the possible dynamic processes that might be leading to non-repeatability.

REFERENCES

[1] Allan, K.M. Laminar Smoke Points of Candle Flames. University of Maryland, College Park. 2007.

[2] Hamins, A., Bundy, M., Dillon, S. Characterization of Candle Flames. Journal of Fire Protection Engineering, Vol. 15. Society of Fire Protection Engineers. November 2005.

[3] Viegas, D. Forest Fire Propagation. Philosophical Transactions: Mathematical, Physical and Engineering Sciences, Vol. 356, No. 1748, Fire Dynamics. The Royal Society. December 15, 1998.

[4] Battaglia, F., Rehm, R., Baum, H. The Fluid Mechanics of Fire Whirls: An Iniscid Model. Physics of Fluids, Vol. 12, No. 11. American Institute of Physics. November 2000.

[5] Farhloul, M., Nicaise, S., Paquet, L. A Mixed Formulation of Boussinesq Equations: Analysis of Nonsingular Solutions. Mathematics of Computation, Vol. 69, No. 231. American Mathematical Society. March 3, 2000.

[6] Kaper, H.G., Leaf, G.K., Matkowsky, B.J., Olmstead, W.E. Dynamics of Nonadiabatic Premixed Flames in a Gravitational Feild. SIAM Journal of Applied Mathematics, Vol. 47, No. 3. Society for Industrial and Applied Mathematics. June 1987.

[7] Candle Making and Ingredients. National Candle Association. Washington, DC. 2002.

[8] Cote, A.E., Linville, J., eds. Fire Protection Handbook, 17th Ed. National Fire Protection Association. Quincy, MA. 1991.

[9] Weast, R.C., ed. CRC Handbook of Chemistry and Physics, 64th Ed. (1983-1984). CRC Press. 1983.

[10] Liepmann, H.W., Roshko, A. Elements of Gas Dynamics. Dover Publications, Inc. Mineola, New York. 2001.

[11] Faber, T.E. Fluid Dynamics for Physicists. Cambridge University Press. New York, NY. 1995.

[12] McGrattan, K., Baum, H., Rehm, R., Mell, W., McDermott, R., Hostikka, S., Floyd, J. Fire Dynamics Simulator (Version 5.5): Technical Reference Guide, Vol. 1: Mathematical Model. National Institute of Standards and Technology. October, 29, 2010.

[13] Bowen, R.M., Wang, C.-C. Introduction to Vectors and Tensors. Dover Publications, Inc. Mineola, NY. 2008.

[14] Xue, H., Ho, J.C., Cheng, Y.M. Comparison of Different Combustion Models in Enclosure Fire Simulation. Fire Safety Journal, Vol. 36. Elsevier. 2001.

[15] Hua, J., Kumar, K., Khoo, B.C., Xue, H. A Numerical Study of the Interaction of Water Spray with a Fire Plume. Fire Safety Journal, Vol. 37. Elsevier. 2002.

[16] Coanda Effect. Wikipedia. http://en.wikipedia.org/wiki/Coanda_effect . Retreived September 5, 2011.

[17] King's Cross Fire. Wikipedia. http://en.wikipedia.org/wiki/King's_Cross_fire . Retrieved September 5, 2011.

[18] Wu, Y., Drysdale, D.D. Study of Upward Flame Spread on Inclined Surfaces. HSE Contract Research Report, No. 122/1996. Health and Safety Executive. 1996.

[19] Heskestad, G. Dynamics of the Fire Plume. Philosophical Transactions: Mathematical, Physical and Engineering Sciences, Vol. 356, No. 1748, Fire Dynamics. The Royal Society. December 15, 1998.

Appendix A. Code

```c
#include <stdio.h>

#include <math.h>

#include <stdlib.h>


#define XMAX 11

#define YMAX 8

#define TMAX 1000

#define XCAN 5

/* location of candle in X */

#define YCAN 1

/* location of candle on y-axis.  */




const double ystep = 3.5;                    /* cm */

const double xstep = 3.18;

const int tstep = 1.0;          /* sec. */



const double difcon = 0.1*1.0/3.18/3.5; /* unitless. */

const double o2init = 21.0;/* percent o2 as
```

```c
                                                    read by meter */
const double br_to_dbar = 1.2;


prnt_o2(double o2[XMAX][YMAX][TMAX], int t)
{
    int x,y;
    printf("---------t = %i ------------\n", t);
    for(y=YMAX-1;y>=0;y--) {
        for(x=0;x<XMAX;x++)
            printf("%lf\t", o2[x][y][t]);
        putchar('\n');
    }
    printf("---------------------\n");
}


int diffuse(double o2[XMAX][YMAX][TMAX], int t, double br)
{
    int x,y,q,p;
    double dbar;
```

```
for (x=0;x<XMAX;x++)

    for (y=0;y<YMAX;y++)

        o2[x][y][t+1] = o2[x][y][t];  /* copy from

                                                     prior time */



dbar = br*br_to_dbar;                    /* dbar is the length of the

                                         cell from which o2 moves to

                                                     adjacent cell */

if (dbar > ystep)

    dbar = ystep;                        /* can't move more then

                                         entire cell contents. */

if (dbar > xstep)

    dbar = xstep;



x=XCAN;                                  /* Central column */

for (y=0;y<(YMAX-1);y++) {

    o2[x][y+1][t+1] += dbar/ystep*o2[x][y][t];
```

```
      o2[x][y][t+1]    -= dbar/ystep*o2[x][y][t];

}

dbar /=2.0;                        /* Now we are OUT of central

                                   column and HALF goes

                                        each way. */

y=YMAX-1;                          /* roof of container. */

for(x=XCAN;x<XMAX-1;x++) {         /* right half of

                                        ceiling */

   o2[x+1][y][t+1] +=  dbar/xstep*o2[x][y][t];

   o2[x][y][t+1]    -= dbar/xstep*o2[x][y][t];

}

for(x=XCAN;x>0;x--) { /* left half ceiling */

   o2[x-1][y][t+1] +=  dbar/xstep*o2[x][y][t];

   o2[x][y][t+1]    -= dbar/xstep*o2[x][y][t];

}

x=0;

for(y=YMAX-1;y>0;y--) {            /* x=0 (left) wall */

   o2[x][y-1][t+1] += dbar/ystep*o2[x][y][t];

   o2[x][y][t+1]    -= dbar/ystep*o2[x][y][t];
```

```
}
x=XMAX-1;
for(y=YMAX-1;y>0;y--) {            /* x=XMAX-1 (right) wall */
   o2[x][y-1][t+1] += dbar/ystep*o2[x][y][t];
   o2[x][y][t+1]   -= dbar/ystep*o2[x][y][t];
}
y=0;
for(x=0;x<XCAN;x++) {
   o2[x+1][y][t+1] += dbar/xstep*o2[x][y][t];
   o2[x][y][t+1] -= dbar/xstep*o2[x][y][t];
}
for(x=XMAX-1;x>XCAN;x--) {
   o2[x-1][y][t+1] += dbar/xstep*o2[x][y][t];
   o2[x][y][t+1] -= dbar/xstep*o2[x][y][t];
}
//   prnt_o2(o2,t+1);
for(x=0;x<XMAX;x++)
   for(y=0;y<YMAX;y++) {
      for(q=x-1;q<=x+1;q++) {    /* q has to be x-1, x
```

```c
                                              and x+1 only. */

        p=y;

        if (!((q<0) || (q>=XMAX))) {

            o2[x][y][t+1] -= difcon * (o2[x][y][t]-o2[q][p][t]);

            o2[q][p][t+1] += difcon * (o2[x][y][t]-o2[q][p][t]);

        }

    }

    for (p=y-1;p<=y+1;p++) {

        q=x;

        if (!((p<0) || (p>=YMAX))) {

            o2[x][y][t+1] -= difcon * (o2[x][y][t]-o2[q][p][t]);

            o2[q][p][t+1] += difcon * (o2[x][y][t]-o2[q][p][t]);

        }

    }

}
//  prnt_o2(o2, t+1);

}
```

```c
int main()
{
    double o2[XMAX][YMAX][TMAX];
    int t;                                   /* time in units of tstep? */
    int x,y;
    double br, o2i;
    const double br_max = 0.285;
    const double o2_min = 14.0;
    FILE * fout;
    fout = fopen("output.txt","wt");


    /* initialize O2 to be starting value */
    //   o2i = o2init;
    for (x=0;x<XMAX;x++)
      for (y=0;y<YMAX;y++)
        o2[x][y][0] = o2init;
    //   prnt_o2(o2,0);
    for (t=0;t<TMAX-100;t++) {
        br = br_max * (o2[XCAN][YCAN][t] - o2_min);
```

```c
    if (br < 0.0)

        br = 0.0;                          /* don't allow spontanious

                                              creation of o2! */

    o2[XCAN][YCAN][t] -= br;              /* subtract burt o2

                                              from candle area */

    diffuse(o2, t, br);

    //      prnt_o2(o2, t);

    //      prnt_o2(o2, t+1);

    if ((t%10) == 0) {

        fprintf(fout, "%i LL %2.2lf ML %2.2lf UL %2.2lf UR %2.2lf

            CO %2.2lf CAN %2.2lf BR %2.2lf \n", t, o2[0][0][t], o2[0]

            [(int)YMAX/2][t], o2[0][YMAX-1][t], o2[XMAX-1][YMAX-1][t],

            o2[XCAN][0][t], o2[XCAN][YCAN][t], br);

        fflush(fout);

    }

    printf("%i\n", t);

    }

    fclose(fout);

}
```

Appendix B. Code Output

Total percent O_2 within container as a function of time.

0 21.000000 21.000000 21.000000 21.000000 20.400000

10 20.922912 20.516050 20.517729 20.863699 18.701036

20 20.698123 20.076110 20.073728 20.531883 18.350653

30 20.418932 19.732981 19.721008 20.189365 18.125902

40 20.130076 19.442009 19.422984 19.877113 17.936848

50 19.847749 19.181325 19.158826 19.592382 17.766117

60 19.577494 18.941252 18.917618 19.328994 17.608035

70 19.320907 18.717266 18.693736 19.082963 17.460132

80 19.078113 18.507012 18.484183 18.851952 17.321109

90 18.848698 18.309085 18.287218 18.634487 17.190156

100 18.632063 18.122515 18.101708 18.429515 17.066683

110 18.427556 17.946544 17.926813 18.236203 16.950212

120 18.234526 17.780521 17.761847 18.053832 16.840323

130 18.052345 17.623865 17.606210 17.881760 16.736633

140 17.880410 17.476040 17.459359 17.719392 16.638788

150 17.718152 17.336544 17.320790 17.566178 16.546458

160 17.565027 17.204907 17.190032 17.421598 16.459331

170 17.420525 17.080685 17.066643 17.285165 16.377112

180 17.284160 16.963462 16.950207 17.156418 16.299526

190 17.155476 16.852842 16.840332 17.034926 16.226311

200 17.034041 16.748454 16.736647 16.920279 16.157221

210 16.919446 16.649948 16.638804 16.812091 16.092024

220 16.811306 16.556991 16.546474 16.709998 16.030499

230 16.709259 16.469270 16.459346 16.613657 15.972441

240 16.612960 16.386492 16.377127 16.522744 15.917654

250 16.522087 16.308378 16.299540 16.436954 15.865954

260 16.436334 16.234665 16.226324 16.355996 15.817166

270 16.355411 16.165104 16.157234 16.279600 15.771127

280 16.279048 16.099462 16.092035 16.207507 15.727682

290 16.206987 16.037519 16.030510 16.139477 15.686685

300 16.138986 15.979066 15.972452 16.075279 15.647997

310 16.074816 15.923905 15.917664 16.014698 15.611489

320 16.014261 15.871853 15.865963 15.957530 15.577038

330 15.957118 15.822733 15.817175 15.903584 15.544528

340 15.903194 15.776381 15.771136 15.852676 15.513850

350 15.852309 15.732640 15.727690 15.804636 15.484900

360 15.804290 15.691363 15.686692 15.759304 15.457580

370 15.758976 15.652412 15.648004 15.716525 15.431801

380 15.716216 15.615655 15.611496 15.676156 15.407473

390 15.675865 15.580969 15.577045 15.638061 15.384516

400 15.637787 15.548238 15.544534 15.602113 15.362853

410 15.601854 15.517350 15.513855 15.568190 15.342410

420 15.567946 15.488203 15.484905 15.536179 15.323118

430 15.535948 15.460698 15.457585 15.505971 15.304914

440 15.505753 15.434742 15.431805 15.477464 15.287735

450 15.477259 15.410249 15.407477 15.450564 15.271524

460 15.450370 15.387136 15.384520 15.425180 15.256227

470 15.424996 15.365324 15.362857 15.401225 15.241791

480 15.401052 15.344742 15.342413 15.378620 15.228169

490 15.378457 15.325320 15.323122 15.357289 15.215314

500 15.357135 15.306991 15.304917 15.337159 15.203183

510 15.337014 15.289695 15.287738 15.318164 15.191736

520 15.318027 15.273374 15.271527 15.300239 15.180933

530 15.300109 15.257972 15.256230 15.283323 15.170740

540 15.283201 15.243438 15.241794 15.267361 15.161120

550 15.267246 15.229723 15.228171 15.252298 15.152043

560 15.252189 15.216780 15.215316 15.238084 15.143477

570 15.237981 15.204567 15.203185 15.224670 15.135393

580 15.224573 15.193042 15.191738 15.212012 15.127765

590 15.211921 15.182166 15.180935 15.200068 15.120567

600 15.199981 15.171903 15.170742 15.188796 15.113774

610 15.188714 15.162218 15.161122 15.178159 15.107364

620 15.178082 15.153079 15.152044 15.168122 15.101315

630 15.168049 15.144454 15.143478 15.158650 15.095607

640 15.158581 15.136316 15.135395 15.149711 15.090221

650 15.149647 15.128636 15.127767 15.141277 15.085138

660 15.141216 15.121388 15.120568 15.133317 15.080341

670 15.133260 15.114549 15.113776 15.125806 15.075815

680 15.125752 15.108096 15.107365 15.118718 15.071543

690 15.118667 15.102006 15.101317 15.112030 15.067513

700 15.111982 15.096259 15.095608 15.105718 15.063709

710 15.105673 15.090836 15.090222 15.099762 15.060120

720 15.099719 15.085718 15.085139 15.094141 15.056733

730 15.094101 15.080889 15.080342 15.088838 15.053536

740 15.088799 15.076331 15.075816 15.083832 15.050520

750 15.083796 15.072031 15.071544 15.079109 15.047674

760 15.079075 15.067973 15.067513 15.074652 15.044988

770 15.074620 15.064143 15.063710 15.070446 15.042453

780 15.070416 15.060529 15.060120 15.066478 15.040061

790 15.066449 15.057119 15.056733 15.062732 15.037804

800 15.062705 15.053901 15.053537 15.059198 15.035675

810 15.059172 15.050864 15.050521 15.055863 15.033665

820 15.055839 15.047999 15.047674 15.052715 15.031768

830 15.052693 15.045294 15.044988 15.049745 15.029978

840 15.049724 15.042742 15.042454 15.046943 15.028289

850 15.046923 15.040334 15.040062 15.044298 15.026695

860 15.044279 15.038062 15.037805 15.041802 15.025191

870 15.041784 15.035918 15.035675 15.039447 15.023772

880 15.039430 15.033894 15.033665 15.037225 15.022433

890 15.037209 15.031984 15.031768 15.035128 15.021169

900 15.035112 15.030182 15.029979 15.033148 15.019976

910 15.033134 15.028482 15.028290 15.031281 15.018851

920 15.031267 15.026877 15.026696 15.029519 15.017789

930 15.029506 15.025363 15.025192 15.027855 15.016787

940 15.027843 15.023934 15.023772 15.026286 15.015841

950 15.026275 15.022586 15.022433 15.024805 15.014948

960 15.024794 15.021313 15.021169 15.023408 15.014106

970 15.023398 15.020112 15.019977 15.022089 15.013311

980 15.022079 15.018979 15.018851 15.020844 15.012561

990 15.020835 15.017910 15.017789 15.019670 15.011854

Indication of percent O_2 as a function of time at the placement of the candle (CAN), the Upper Left region (UL), Middle Left region (ML), Lower Left region (LL), Upper Right region (UR), etc. of the container.

0 LL 21.00 ML 21.00 UL 21.00 UR 21.00 C0 21.00 CAN 19.00 BR 1.99

10 LL 19.13 ML 22.13 UL 22.48 UR 22.48 C0 22.43 CAN 19.91 BR 2.36

20 LL 19.84 ML 21.85 UL 20.81 UR 20.81 C0 21.39 CAN 18.71 BR 1.88

30 LL 19.76 ML 20.90 UL 20.47 UR 20.47 C0 21.75 CAN 18.88 BR 1.95

40 LL 19.11 ML 20.42 UL 19.85 UR 19.85 C0 21.80 CAN 19.07 BR 2.02

50 LL 18.67 ML 19.95 UL 19.67 UR 19.67 C0 21.29 CAN 18.63 BR 1.84

60 LL 18.33 ML 19.82 UL 19.69 UR 19.69 C0 20.87 CAN 18.22 BR 1.68

70 LL 18.16 ML 19.77 UL 19.54 UR 19.54 C0 20.55 CAN 17.90 BR 1.56

80 LL 18.09 ML 19.64 UL 19.32 UR 19.32 C0 20.33 CAN 17.67 BR 1.46

90 LL 18.00 ML 19.46 UL 19.11 UR 19.11 C0 20.20 CAN 17.53 BR 1.41

100 LL 17.86 ML 19.27 UL 18.91 UR 18.91 C0 20.10 CAN 17.43 BR 1.37

110 LL 17.71 ML 19.09 UL 18.75 UR 18.75 C0 19.97 CAN 17.31 BR 1.32

120 LL 17.56 ML 18.93 UL 18.61 UR 18.61 C0 19.83 CAN 17.18 BR 1.27

130 LL 17.43 ML 18.79 UL 18.50 UR 18.50 C0 19.68 CAN 17.05 BR 1.21

140 LL 17.30 ML 18.68 UL 18.40 UR 18.40 C0 19.54 CAN 16.91 BR 1.16

150 LL 17.19 ML 18.57 UL 18.30 UR 18.30 C0 19.40 CAN 16.78 BR 1.11

160 LL 17.09 ML 18.47 UL 18.20 UR 18.20 C0 19.28 CAN 16.67 BR 1.06

170 LL 17.00 ML 18.37 UL 18.10 UR 18.10 C0 19.16 CAN 16.56 BR 1.02

180 LL 16.91 ML 18.28 UL 18.01 UR 18.01 C0 19.05 CAN 16.46 BR 0.98

190 LL 16.83 ML 18.19 UL 17.93 UR 17.93 C0 18.95 CAN 16.36 BR 0.94

200 LL 16.74 ML 18.10 UL 17.84 UR 17.84 C0 18.85 CAN 16.28 BR 0.91

210 LL 16.66 ML 18.01 UL 17.76 UR 17.76 C0 18.76 CAN 16.19 BR 0.87

220 LL 16.59 ML 17.93 UL 17.69 UR 17.69 C0 18.67 CAN 16.11 BR 0.84

230 LL 16.51 ML 17.85 UL 17.61 UR 17.61 C0 18.58 CAN 16.03 BR 0.81

240 LL 16.44 ML 17.77 UL 17.55 UR 17.55 C0 18.50 CAN 15.95 BR 0.78

250 LL 16.37 ML 17.70 UL 17.48 UR 17.48 C0 18.41 CAN 15.88 BR 0.75

260 LL 16.30 ML 17.63 UL 17.42 UR 17.42 C0 18.33 CAN 15.81 BR 0.72

270 LL 16.24 ML 17.56 UL 17.36 UR 17.36 C0 18.25 CAN 15.74 BR 0.69

280 LL 16.17 ML 17.50 UL 17.30 UR 17.30 C0 18.17 CAN 15.68 BR 0.67

290 LL 16.11 ML 17.44 UL 17.25 UR 17.25 C0 18.10 CAN 15.61 BR 0.64

300 LL 16.06 ML 17.38 UL 17.20 UR 17.20 C0 18.03 CAN 15.55 BR 0.62

310 LL 16.00 ML 17.32 UL 17.15 UR 17.15 C0 17.96 CAN 15.50 BR 0.60

320 LL 15.95 ML 17.26 UL 17.10 UR 17.10 C0 17.89 CAN 15.44 BR 0.57

330 LL 15.89 ML 17.21 UL 17.06 UR 17.06 C0 17.82 CAN 15.39 BR 0.55

340 LL 15.84 ML 17.16 UL 17.02 UR 17.02 C0 17.75 CAN 15.33 BR 0.53

350 LL 15.80 ML 17.11 UL 16.98 UR 16.98 C0 17.69 CAN 15.29 BR 0.51

360 LL 15.75 ML 17.06 UL 16.94 UR 16.94 C0 17.63 CAN 15.24 BR 0.49

370 LL 15.70 ML 17.01 UL 16.90 UR 16.90 C0 17.57 CAN 15.19 BR 0.47

380 LL 15.66 ML 16.96 UL 16.86 UR 16.86 C0 17.51 CAN 15.15 BR 0.46

390 LL 15.62 ML 16.92 UL 16.83 UR 16.83 C0 17.45 CAN 15.10 BR 0.44

400 LL 15.58 ML 16.88 UL 16.80 UR 16.80 C0 17.39 CAN 15.06 BR 0.42

410 LL 15.54 ML 16.83 UL 16.77 UR 16.77 C0 17.33 CAN 15.02 BR 0.41

420 LL 15.50 ML 16.79 UL 16.74 UR 16.74 C0 17.28 CAN 14.99 BR 0.39

430 LL 15.46 ML 16.75 UL 16.71 UR 16.71 C0 17.23 CAN 14.95 BR 0.38

440 LL 15.42 ML 16.72 UL 16.68 UR 16.68 C0 17.17 CAN 14.92 BR 0.37

450 LL 15.39 ML 16.68 UL 16.66 UR 16.66 C0 17.12 CAN 14.88 BR 0.35

460 LL 15.36 ML 16.64 UL 16.63 UR 16.63 C0 17.07 CAN 14.85 BR 0.34

470 LL 15.32 ML 16.61 UL 16.61 UR 16.61 C0 17.02 CAN 14.82 BR 0.33

480 LL 15.29 ML 16.57 UL 16.58 UR 16.58 C0 16.97 CAN 14.79 BR 0.31

490 LL 15.26 ML 16.54 UL 16.56 UR 16.56 C0 16.92 CAN 14.76 BR 0.30

500 LL 15.23 ML 16.51 UL 16.54 UR 16.54 C0 16.87 CAN 14.73 BR 0.29

510 LL 15.20 ML 16.47 UL 16.52 UR 16.52 C0 16.83 CAN 14.71 BR 0.28

520 LL 15.18 ML 16.44 UL 16.50 UR 16.50 C0 16.78 CAN 14.68 BR 0.27

530 LL 15.15 ML 16.41 UL 16.48 UR 16.48 C0 16.74 CAN 14.66 BR 0.26

540 LL 15.13 ML 16.38 UL 16.46 UR 16.46 C0 16.69 CAN 14.64 BR 0.25

550 LL 15.10 ML 16.35 UL 16.44 UR 16.44 C0 16.65 CAN 14.61 BR 0.24

560 LL 15.08 ML 16.32 UL 16.42 UR 16.42 C0 16.60 CAN 14.59 BR 0.24

570 LL 15.05 ML 16.30 UL 16.41 UR 16.41 C0 16.56 CAN 14.57 BR 0.23

580 LL 15.03 ML 16.27 UL 16.39 UR 16.39 C0 16.52 CAN 14.55 BR 0.22

590 LL 15.01 ML 16.24 UL 16.37 UR 16.37 C0 16.48 CAN 14.54 BR 0.21

600 LL 14.99 ML 16.21 UL 16.36 UR 16.36 C0 16.44 CAN 14.52 BR 0.21

610 LL 14.97 ML 16.19 UL 16.34 UR 16.34 C0 16.40 CAN 14.50 BR 0.20

620 LL 14.95 ML 16.16 UL 16.33 UR 16.33 C0 16.36 CAN 14.49 BR 0.19

630 LL 14.93 ML 16.14 UL 16.31 UR 16.31 C0 16.32 CAN 14.47 BR 0.19

640 LL 14.91 ML 16.11 UL 16.30 UR 16.30 C0 16.28 CAN 14.45 BR 0.18

650 LL 14.90 ML 16.09 UL 16.28 UR 16.28 C0 16.25 CAN 14.44 BR 0.18

660 LL 14.88 ML 16.06 UL 16.27 UR 16.27 C0 16.21 CAN 14.43 BR 0.17

670 LL 14.86 ML 16.04 UL 16.25 UR 16.25 C0 16.18 CAN 14.41 BR 0.17

680 LL 14.85 ML 16.02 UL 16.24 UR 16.24 C0 16.14 CAN 14.40 BR 0.16

690 LL 14.83 ML 16.00 UL 16.22 UR 16.22 C0 16.11 CAN 14.39 BR 0.16

700 LL 14.82 ML 15.97 UL 16.21 UR 16.21 C0 16.07 CAN 14.38 BR 0.15

710 LL 14.81 ML 15.95 UL 16.20 UR 16.20 C0 16.04 CAN 14.37 BR 0.15

720 LL 14.79 ML 15.93 UL 16.18 UR 16.18 C0 16.01 CAN 14.36 BR 0.14

730 LL 14.78 ML 15.91 UL 16.17 UR 16.17 C0 15.98 CAN 14.35 BR 0.14

740 LL 14.77 ML 15.89 UL 16.15 UR 16.15 C0 15.94 CAN 14.34 BR 0.13

750 LL 14.75 ML 15.87 UL 16.14 UR 16.14 C0 15.91 CAN 14.33 BR 0.13

760 LL 14.74 ML 15.85 UL 16.13 UR 16.13 C0 15.88 CAN 14.32 BR 0.13

770 LL 14.73 ML 15.83 UL 16.11 UR 16.11 C0 15.85 CAN 14.31 BR 0.12

780 LL 14.72 ML 15.81 UL 16.10 UR 16.10 C0 15.83 CAN 14.30 BR 0.12

790 LL 14.71 ML 15.79 UL 16.09 UR 16.09 C0 15.80 CAN 14.30 BR 0.12

800 LL 14.70 ML 15.77 UL 16.08 UR 16.08 C0 15.77 CAN 14.29 BR 0.12

810 LL 14.69 ML 15.75 UL 16.06 UR 16.06 C0 15.74 CAN 14.28 BR 0.11

820 LL 14.68 ML 15.73 UL 16.05 UR 16.05 C0 15.72 CAN 14.27 BR 0.11

830 LL 14.67 ML 15.71 UL 16.04 UR 16.04 C0 15.69 CAN 14.27 BR 0.11

840 LL 14.66 ML 15.70 UL 16.02 UR 16.02 C0 15.66 CAN 14.26 BR 0.10

850 LL 14.65 ML 15.68 UL 16.01 UR 16.01 C0 15.64 CAN 14.26 BR 0.10

860 LL 14.64 ML 15.66 UL 16.00 UR 16.00 C0 15.62 CAN 14.25 BR 0.10

870 LL 14.63 ML 15.64 UL 15.99 UR 15.99 C0 15.59 CAN 14.24 BR 0.10

880 LL 14.62 ML 15.63 UL 15.97 UR 15.97 C0 15.57 CAN 14.24 BR 0.10

890 LL 14.61 ML 15.61 UL 15.96 UR 15.96 C0 15.55 CAN 14.23 BR 0.09

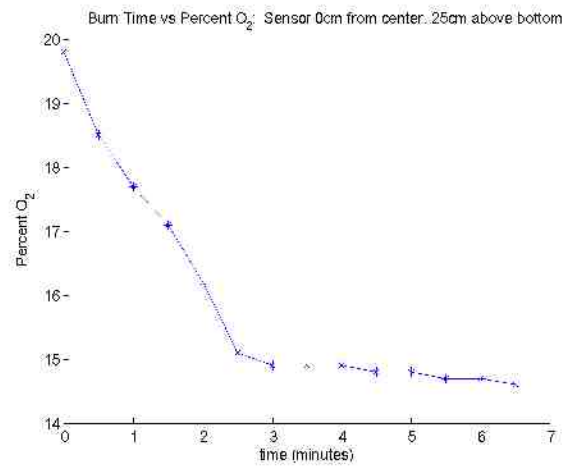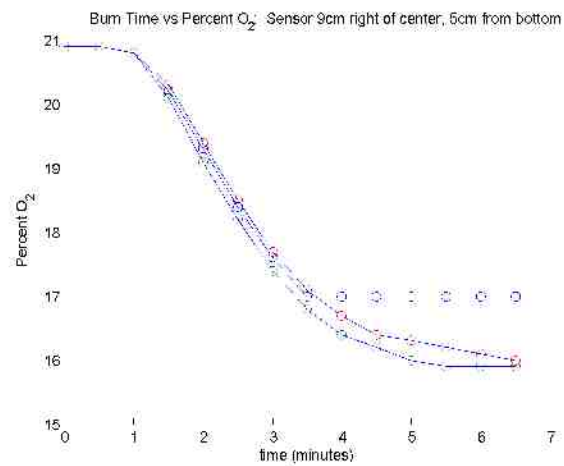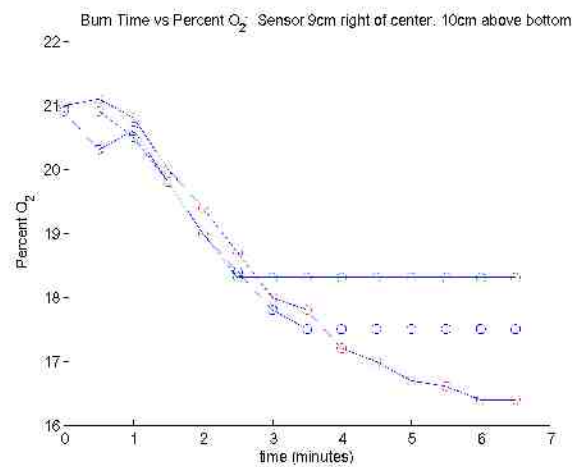APPENDIX C. RESULTS FROM SERIES 1 AND 2
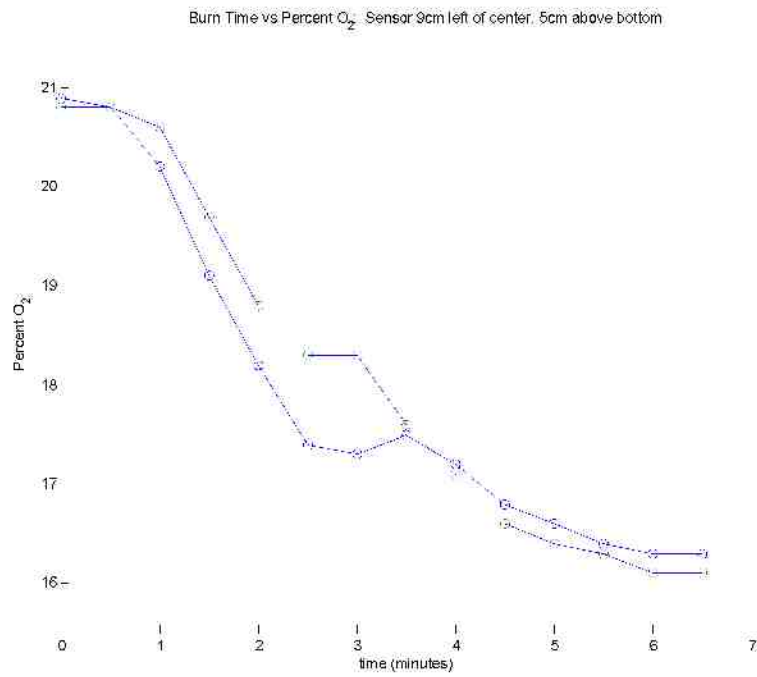
FIGURE 11. Burn time versus percent O_2: Sensor 9cm left of center, 5cm above bottom, series 2.
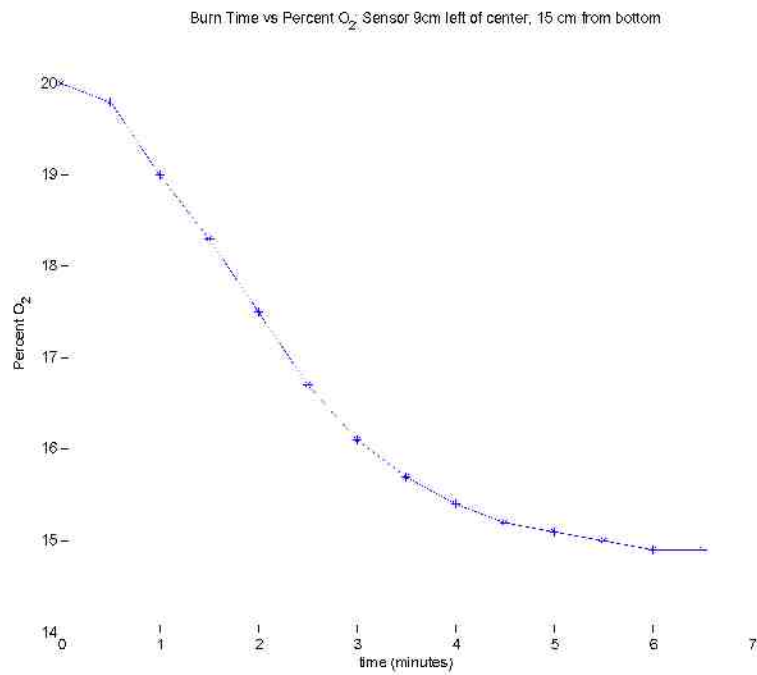
FIGURE 12. Burn time versus percent O_2: Sensor 9cm left of center, 15cm above bottom, series 1.

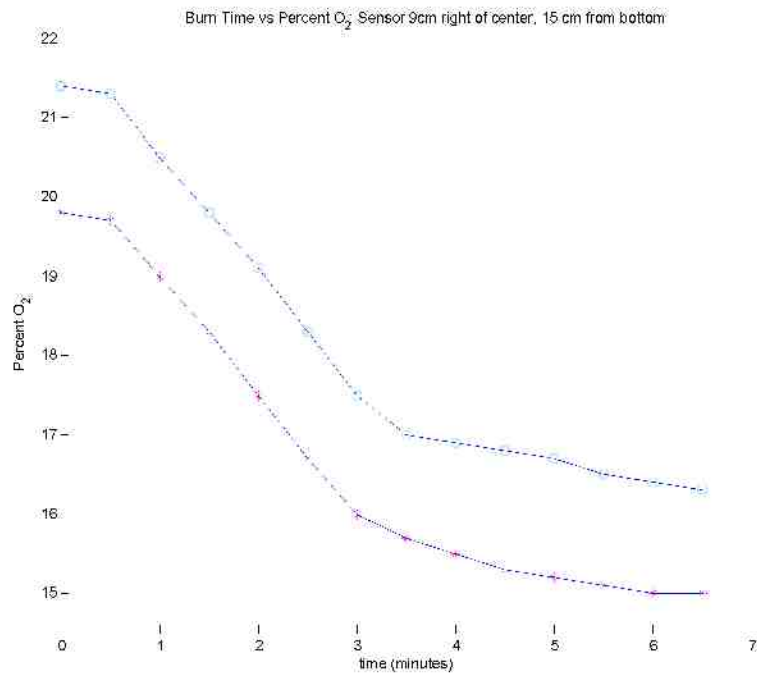Burn Time vs Percent O$_2$: Sensor 9cm left of center, 20 cm above bottom
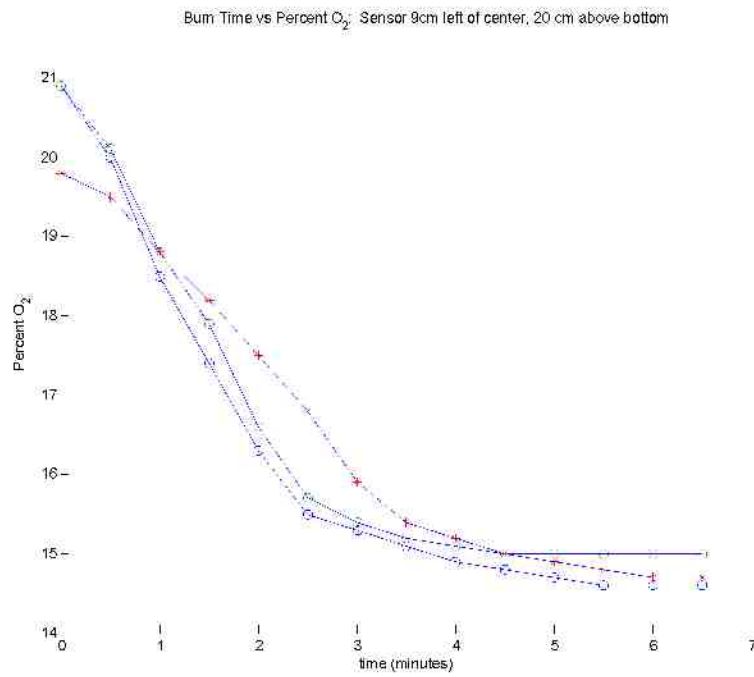
FIGURE 13. Burn time versus percent O$_2$: Sensor 9cm left of center, 20cm above bottom. Cross data points: Series 1. Circular data points: Series 2.

Burn Time vs Percent O$_2$: Sensor 9cm left of center, 25 cm above bottom
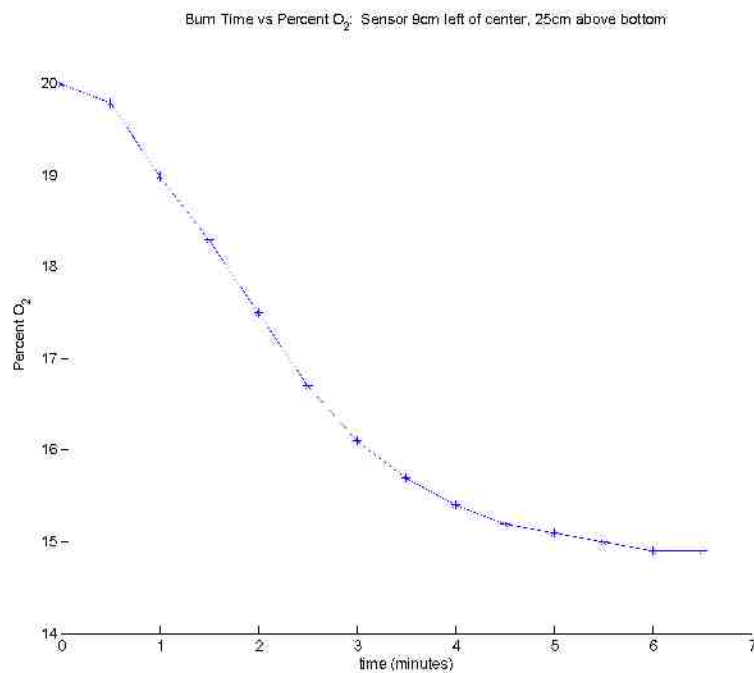
FIGURE 14. Burn time versus percent O$_2$: Sensor 9cm left of center, 25cm above bottom, series 1.
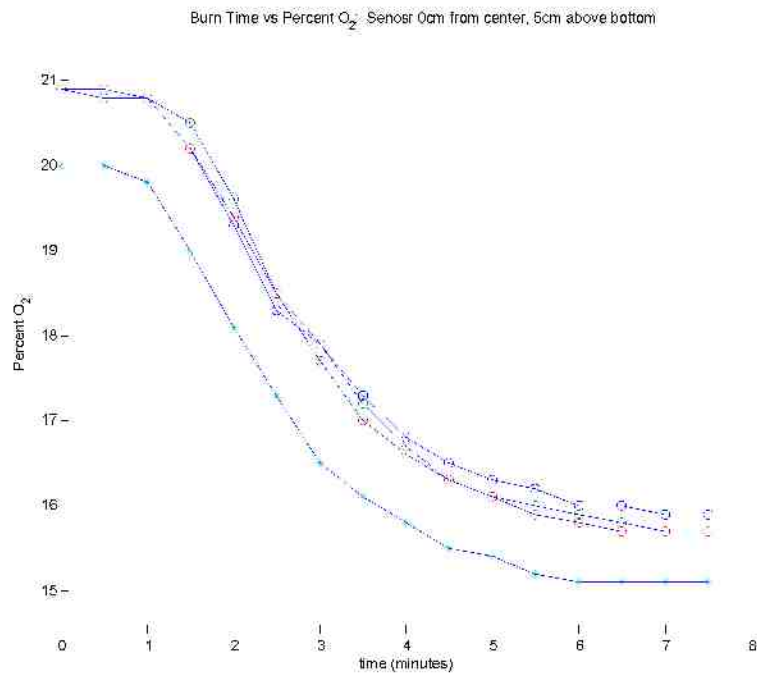
Figure 15. Burn time versus percent O_2: Sensor 0cm right of center, 5cm above bottom. Cross data points: Series 1. Circular data points: Series 2.
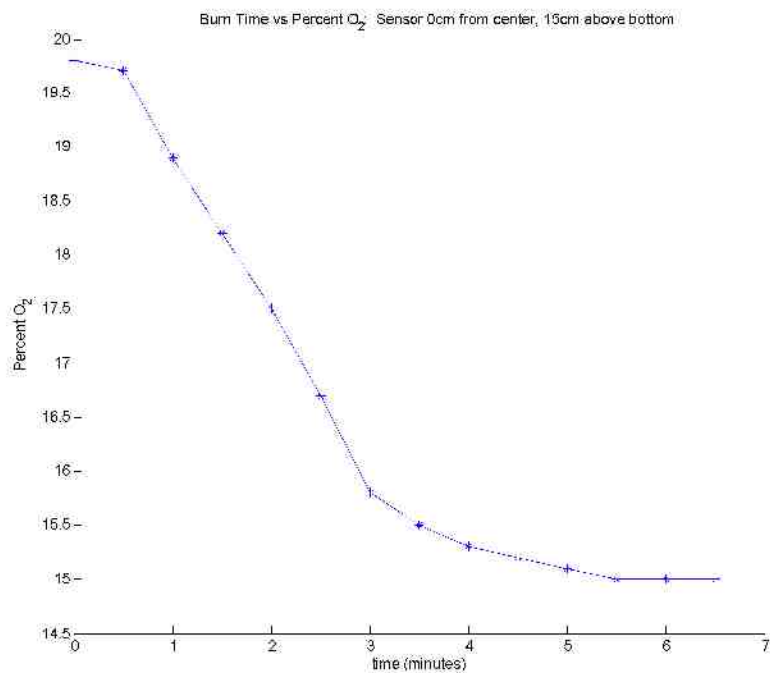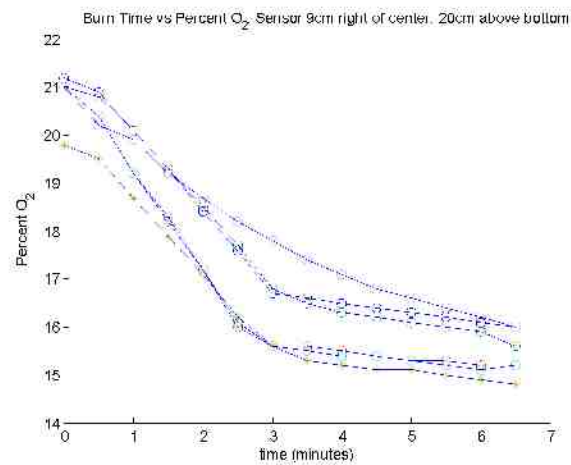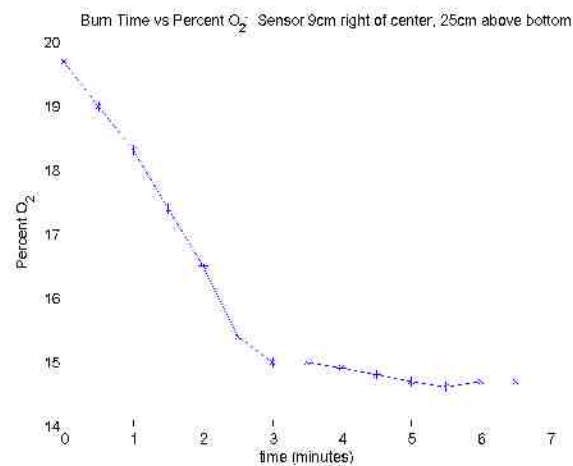

Figure 16. Burn time versus percent O_2: Sensor 0cm right of center, 15cm above bottom, series 1
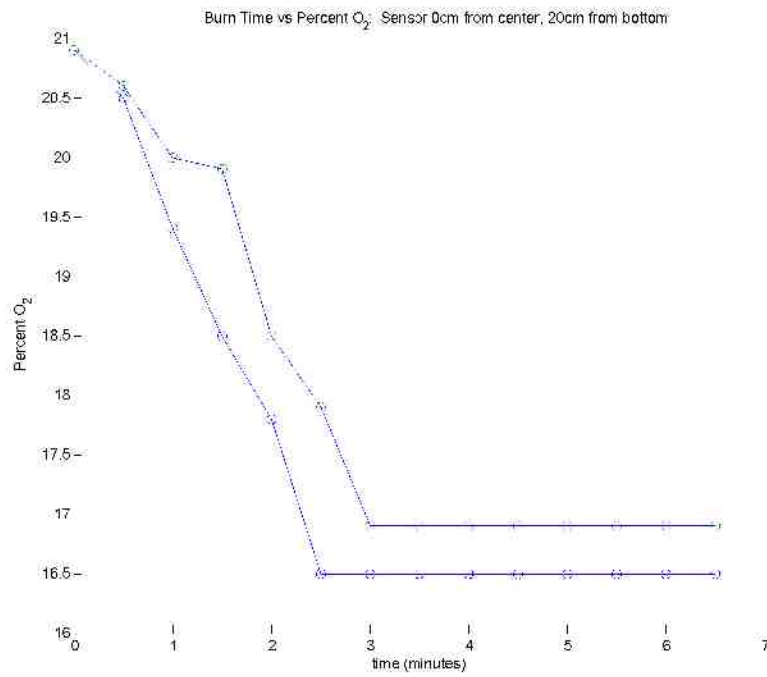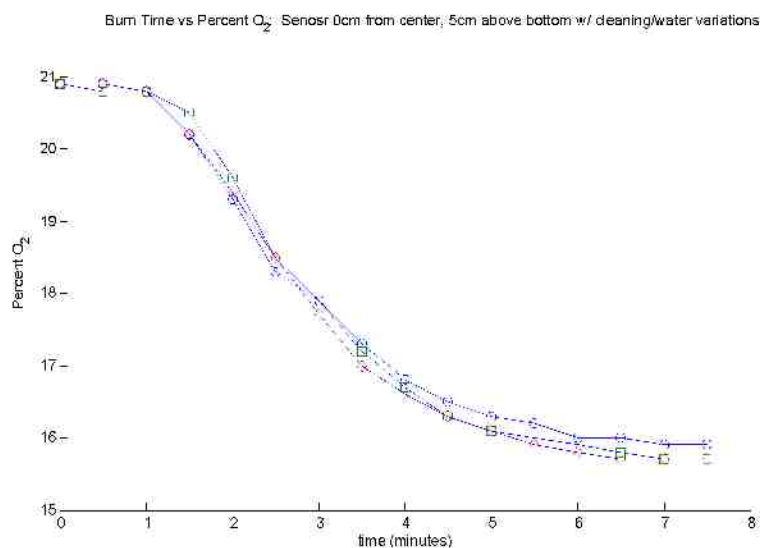
FIGURE 17. Burn time versus percent O_2: Sensor 0cm right of center, 20cm above bottom, series 2.

FIGURE 18. Burn time versus percent O_2: Sensor 0cm right of center, 25cm above bottom, series 1.

FIGURE 19. Burn time versus percent O_2: Sensor 9cm right of center, 5cm above bottom, series 2.

FIGURE 20. Burn time versus percent O_2: Sensor 9cm right of center, 10cm above bottom, series 2.

FIGURE 21. Burn time versus percent O_2: Sensor 9cm right of center, 15cm above bottom. Cross data points: Series 1. Circular data points: Series 2.

FIGURE 22. Burn time versus percent O_2: Sensor 9cm right of center, 20cm above bottom. Cross data points: Series 1. Circular data points: Series 2.

FIGURE 23. Burn time versus percent O_2: Sensor 9cm right of center, 25cm above bottom, series 1.

FIGURE 24. Burn time versus percent O_2: Sensor 0cm right of center, 5cm above bottom with cleaning and water variations. Circle = untouched walls, no water added to top of glass lid. Square = walls wiped down, no water added to glass lid. Diamond = walls wiped down, water added to top of glass lid.
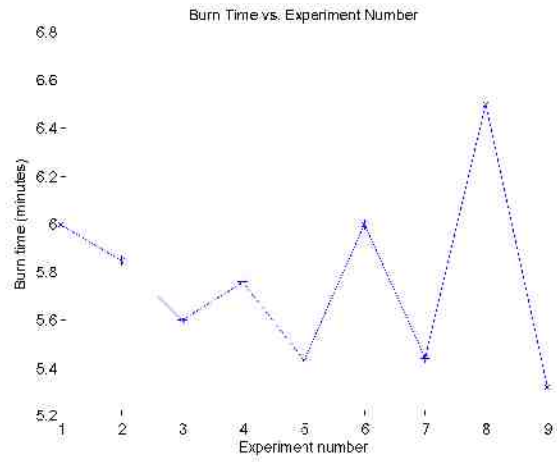
79

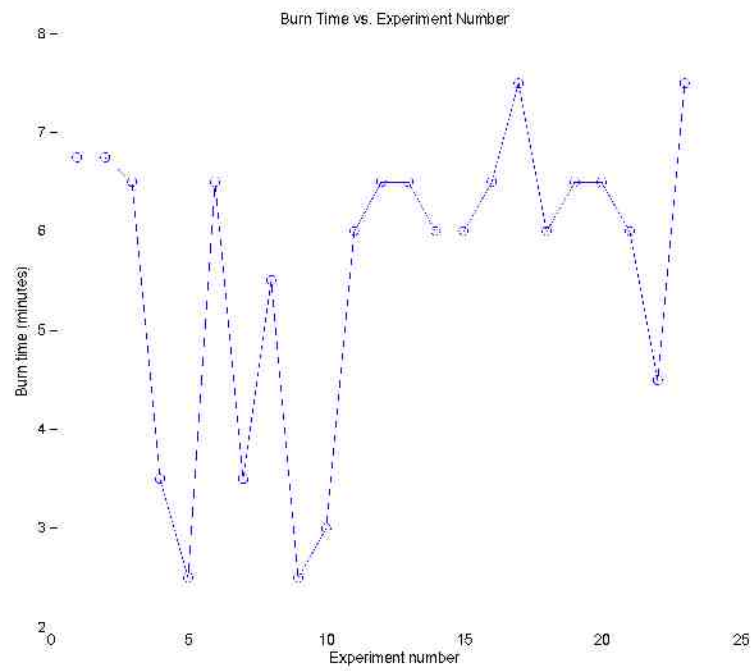FIGURE 25. Burn time versus experiment number, series 1.

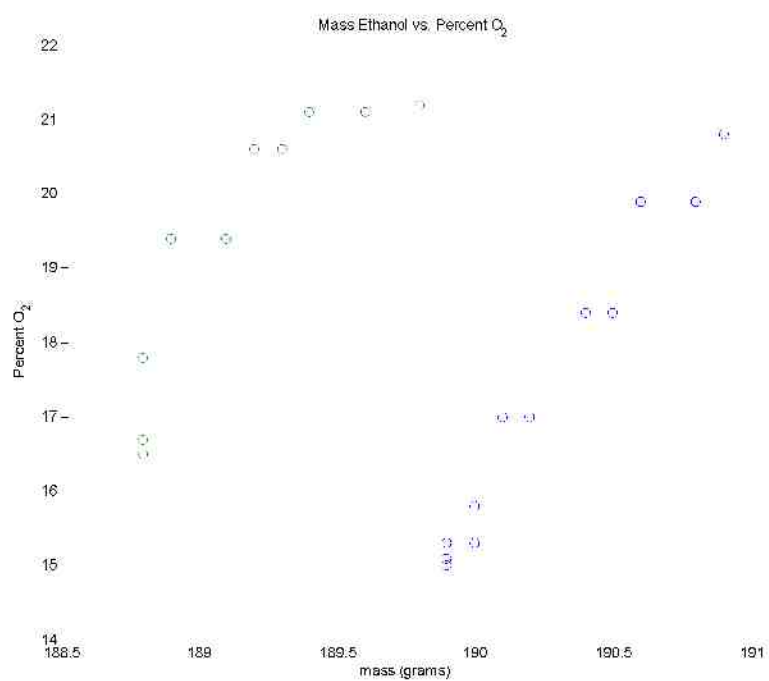FIGURE 26. Burn time versus experiment number, series 1.

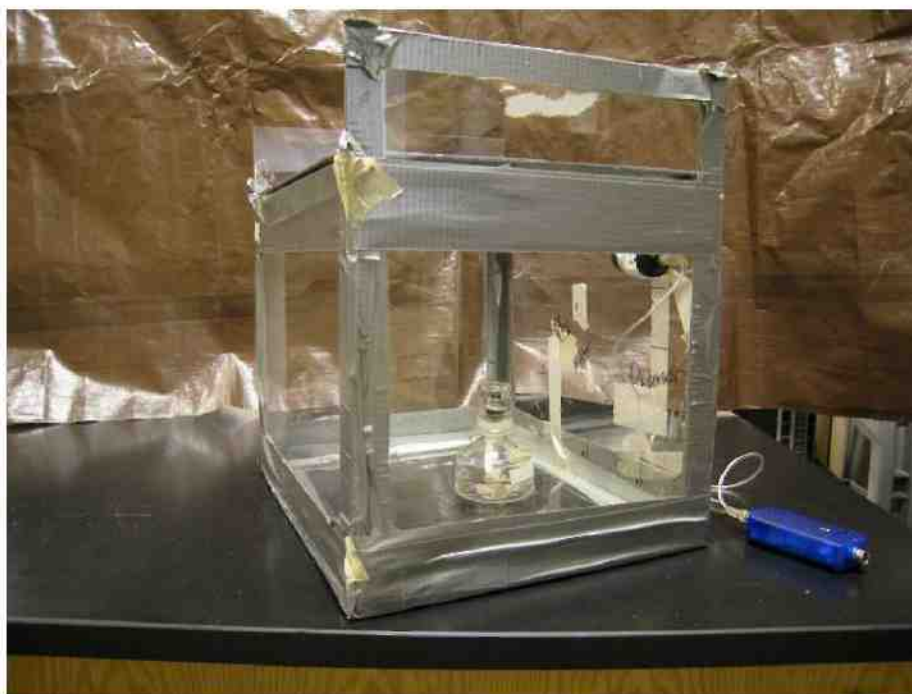Figure 27. Mass of ethanol versus percent O_2, series 2.

Figure 28. Experimental apparatus, external view.

FIGURE 29. Experimental apparatus, internal view.